Neutron scattering and amorphous polymers

Ann Maconnachie
Department of Chemical Engineering and Chemical Technology, Imperial College, London SW7 2BY, UK
and Randal W. Richards
Department of Pure and Applied Chemistry, Strathclyde University, Glasgow G1 1XL, UK
(Received 18 January 1978)

During the past ten years neutron scattering has become a much more widely used technique. The use of neutron scattering to study the conformation and dynamics of polymer chains in the bulk amorphous state and in solution is reviewed here. The basic theory of neutron scattering is introduced. The types of instruments which are currently used and the factors affecting neutron scattering experiments are discussed. The following sections are each concerned with a different type of scattering experiment and the information which has been obtained. At the beginning of each of these sections the theory relating to the particular topic under discussion is introduced. The three topics covered by this review are: conformation studies of polymers; dynamics of polymer chains and studies of side group motion in polymers.

INTRODUCTION

Neutron scattering has been used extensively to investigate the physics of the solid state[1]. During the past ten years the technique has been applied increasingly to chemical problems, a phenomenon due in part to the development of suitable spectrometers. Reviews[2,3] of such applications have recently been published and include studies of hydrogen bonding, covalency, liquid structure and molecular spectroscopy. This review is solely concerned with thermal neutron scattering studies of polymers in the amorphous solid state and in solution.

Thermal neutrons have wavelengths in the range of 2 to 20 Å and energies of between 400 and 0.4 J/mol (20–0.2 meV). It is this combination of properties which makes neutrons so useful in the study of the structure and the dynamic properties of a system. Neutron wavelengths have a magnitude approximately equal to that of interatomic separations whilst neutron energies are of the same order as molecular vibrational energies. The general theory of neutron scattering is set out in the following section and forms the basis for the more detailed treatments in later sections. Examples of the instruments available are discussed in the second section. Also included here are factors which influence the choice of experimental conditions.

Elastic scattering of neutrons measures correlations between scattering centres and for polymers this enables the conformation to be determined. The theory of such small-angle neutron scattering (SANS) is developed in the section on conformation studies and experimental results from a variety of systems are discussed.

When a neutron is scattered by an atom or group undergoing some type of motion then energy can be exchanged between the two interacting species. If the moving atom undergoes diffusive motion then the neutron energy is Doppler-shifted. Since the energy change is small this type of scattering is called quasi-elastic scattering. Neutron quasi-elastic scattering (NQES) studies of polymers in the bulk and in solution have given much new information on the Rouse–Zimm modes of a polymer chain. The detailed theory of this type of scattering and experimental results obtained are set out in the section entitled 'Dynamics of polymer chains'.

If the atom is undergoing quantized motion such as vibrational or rotational transitions then the energy exchange gives rise to discrete peaks in the energy spectrum. Using such neutron incoherent inelastic scattering (NIIS) the vibrational behaviour of side groups on the polymer chain can be studied. A review of the experimental results and their correlation with other studies of side group motion is given in the final Applications section.

THEORY

Introduction

It is not intended to give any detailed derivation of the theory of thermal neutron scattering but rather to introduce the basic equations and concepts which will be used throughout this review. A number of excellent books and review articles already exist which describe the theory in more detail; see, for example, Marshall and Lovesey[4], Turchin[5] and Allen and Higgins[6].

Neutrons can interact with the sample under investigation in two ways. The main interaction is that between the neutron and the nucleus via purely nuclear forces and is called nuclear scattering. The second interaction can occur if there are unpaired electrons present; in this case the magnetic moment of the neutron interacts with the magnetic moment of the unpaired electrons. This type of scattering is called magnetic scattering. The theory described below is concerned solely with nuclear scattering of low energy neutrons (thermal neutron scattering).

The magnitude of the interaction between a neutron and an atom does not follow any simple rule as, for example, in X-ray scattering where the interaction is proportional to the number of electrons in the target. In neutron scattering the magnitude of the interaction is essentially the same for all

0032–3861/78/1907–0739$04.00
© 1978 IPC Business Press Ltd

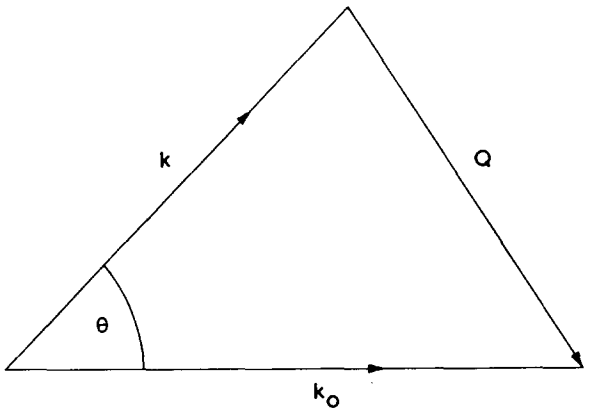

Figure 1 Relationship between the incident wave vector $\mathbf{k}_0$ and the scattered wave vector k where θ is the scattering angle

atoms. Because the neutron interacts with the nucleus, the interaction is different for each isotope as well as each element. The variation in interaction gives rise to incoherent scattering whereas the mean value of the interaction for a particular atom gives rise to coherent scattering.

Momentum and energy transfer

In a scattering experiment the intensity of the scattered beam is measured as a function of energy and/or scattering angle. The vector diagram for a scattering event is shown in *Figure 1*, where $\mathbf{k}_0$ is the incident wave vector, $\mathbf{k}$ is the scattered wave vector and $\mathbf{Q} = \mathbf{k} - \mathbf{k}_0$.

If the incident energy is E_0 and the energy of the scattered neutron is E then the energy transfer is

$$\begin{aligned} E - E_0 &= \Delta E \\ &= \hbar\omega \\ &= \tfrac{1}{2}m(v^2 - v_0^2) \\ &= \frac{\hbar^2}{m}(k^2 - k_0^2) \end{aligned} \tag{1}$$

If the scattering is elastic then no energy change takes place and thus $\Delta E = 0$ and $k = k_0$. In an inelastic scattering event $\Delta E \neq 0$, it can be $<$ or >0 depending upon whether the neutron has gained or lost energy during the scattering event and this depends on the incident energy of the neutron. The momentum transfer is $\hbar\mathbf{Q}$ which can be written as:

$$\hbar\mathbf{Q} = \hbar(k^2 + k_0^2 - 2kk_0\cos\theta)^{1/2} \tag{2}$$

and if $k = k_0$, i.e. the event is elastic then equation (2) becomes the familiar expression

$$Q = |\mathbf{Q}| = \frac{4\pi}{\lambda}\sin\frac{\theta}{2} \quad \text{since } |k_0| = \frac{2\pi}{\lambda} \tag{3}$$

A third form of scattering is called quasi-elastic and this refers to the situation where $\Delta E \to 0$, so that only very small values of ΔE are measured.

Scattering length

The interaction between neutron and nucleus is exceedingly short range, $\sim 10^{-15}$ m, and therefore is very small compared with the wavelength of the neutron, ~1 Å (10^{-10} m). The amplitude of the scattered wave, f, which is isotropic, is equal to $-b$ where b is called the scattering length. b is complex, the real part can be positive or negative and the imaginary part is a measure of the neutron absorption which can occur.

The way in which a neutron interacts with a nucleus depends on their relative spins. If the nucleus has a spin I then the neutron can interact with the nucleus with spin up or down, i.e. in total spin states, T, of $I + \frac{1}{2}$ and $I - \frac{1}{2}$. Associated with these total spin states are scattering lengths b^+ and b^-. The degeneracy of these total spin states is $2T + 1$; therefore there are $2(I + \frac{1}{2}) + 1 = 2(I + 1)$ states associated with b^+ and $2(I - \frac{1}{2}) + 1 = 2I$ states associated with b^-. The total number of states is $2(2I + 1)$ and since the probabilities of each state occurring are identical, then the mean scattering length is:

$$\bar{b} = \frac{I+1}{2I+1}b^+ + \frac{I}{2I+1}b^- \tag{4}$$

and

$$\overline{b^2} = \frac{I+1}{2I+1}|b^+|^2 + \frac{I}{2I+1}|b^-|^2 \tag{5}$$

Equations (4) and (5) hold for an array of nuclei where there is only one isotope with spin I. If there are a number of isotopes each with a different spin then $\bar{b}$ for a particular atom is written as:

$$\bar{b} = \sum_n c_n \frac{I_n + 1}{2I_n + 1} b_n^+ + c_n \frac{I_n}{2I_n + 1} b_n^- \tag{6}$$

where c_n is the concentration of the nth isotope which has scattering lengths b_n^+ and b_n^- associated with it and spin state I_n.

Double differential cross-section

The quantity which will be derived is $d^2\sigma/d\Omega dE$, the double differential cross-section, which is the probability that neutrons will be scattered by an array of N atoms with cross-section σ into solid angle $d\Omega$ with energy change dE. To calculate $d^2\sigma/d\Omega dE$ it is necessary to include various transition probabilities which are brought about by the interaction between the neutron and nucleus. The final form for $d^2\sigma/d\Omega dE$ includes the following components:

(a) the probability that a neutron with wave vector $\mathbf{k}_0$ will be scattered with wave vector $\mathbf{k}$ where $\hat{V}$ is the interaction potential which causes the transition;

(b) the probability that the nucleus will go from initial state λ to final state λ' when it undergoes an inelastic collision with the neutron, in which case

(c) energy must be conserved, i.e.:

Energy gained by the nuclei = $E_{\lambda'} - E_\lambda$

= Energy lost by the neutrons

$= E_0 - E$

$= \hbar\omega$

which is expressed in the cross-section by means of a δ

function, and

(d) the probability that if the initial spin state of the neutron is s the final state will be s'.

The final expression becomes:

$$\frac{d^2\sigma}{d\Omega dE} = \frac{k}{k_0}\left(\frac{m}{2\pi\hbar^2}\right)^2 \sum_{s\lambda} P_\sigma P_\lambda \sum_{s'\lambda'} |\langle ks'\lambda'|\hat{V}|k_0 s\lambda\rangle|^2 \times \delta(\hbar\omega + E_\lambda - E_{\lambda'}) \quad (7)$$

which is called the Born approximation to the cross-section. In order to give the correct form of scattering the Fermi pseudo-potential is used for $\hat{V}$:

$$\hat{V}(\mathbf{r}) = \frac{2\pi\hbar^2}{m}\sum_l b_l \exp(i\mathbf{Q}.\mathbf{R}_l) \quad (8)$$

where $\mathbf{R}_l$ is the position vector of the lth nucleus which has a scattering length b_l. So equation (7) becomes:

$$\frac{d^2\sigma}{d\Omega dE} = \frac{k}{k_0}\sum_{\lambda s} P_s P_\lambda \sum_{s'\lambda'} |\langle s'\lambda'|\sum_l b_l \exp(i\mathbf{Q}.\mathbf{R}_l)|s\lambda\rangle|^2 \times \delta(\hbar\omega + E_\lambda - E_{\lambda'}) \quad (9)$$

Equation (9) is the equation on which neutron scattering theory is based. If the scattering is elastic, equation (9) reduces to:

$$\frac{d\sigma}{d\Omega} = \sum P_\lambda P_s \sum_{l\,l'} \exp[i\mathbf{Q}.(\mathbf{R}_l - \mathbf{R}_l')] \quad \langle s\lambda|b_l^* b_l|s\lambda\rangle \quad (10)$$

where $\mathbf{R}_l$ and $\mathbf{R}_l'$ are the position vectors of two nuclei with scattering lengths b_l and b_l', respectively. If $b_l^* b_l$ is averaged over all random spin orientations and random isotope distributions then equation (10) becomes:

$$\frac{d\sigma}{d\Omega} = \sum_{l,l'} \exp[i\mathbf{Q}.(\mathbf{R}_l - \mathbf{R}_l')] \quad \overline{b_l^* b_{l'}} \quad (11)$$

where

$$\overline{b_l^* b_{l'}} = \sum_\lambda P_\lambda \langle\lambda|b_l^* b_{l'}|\lambda\rangle \quad (12)$$

Now $\overline{b_l^* b_{l'}}$ can be written as:

$$\overline{b_l^* b_{l'}} = \bar{b}^2 + \delta_{l\,l'}(\overline{b^2} - \bar{b}^2) \quad (13)$$

which means that if there is no correlation between the scattering lengths of the l th and l' th nuclei, i.e. $l \neq l'$ then:

$$\overline{b_l^* b_{l'}} = \bar{b}^2$$

but if $l = l'$ then $\overline{b_l^* b_{l'}} = \overline{b^2}$.

Substituting equation (13) into equation (11) gives:

$$\frac{d\sigma}{d\Omega} = \left(\frac{d\sigma}{d\Omega}\right)_{coh} + \left(\frac{d\sigma}{d\Omega}\right)_{inc} \quad (14)$$

where the coherent cross-section:

$$\left(\frac{d\sigma}{d\Omega}\right)_{coh} = \bar{b}^2 \left|\sum_l \exp(i\mathbf{Q}.\mathbf{R}_l)\right|^2 \quad (15)$$

and the incoherent cross-section:

$$\left(\frac{d\sigma}{d\Omega}\right)_{inc} = N[\overline{b^2} - \bar{b}^2] = N\overline{[b - \bar{b}]^2} \quad (16)$$

The incoherent cross-section is isotropic and does not depend on a phase term, therefore no information can be obtained about the relative positions of the nuclei in the array. Information about the relative positions of the nuclei can only be obtained if coherent scattering is measured. The coherent cross-section depends on the mean value of the scattering length and on interference effects between waves scattered from different nuclei.

Incoherent scattering will only occur if there are variations in scattering length away from the mean value. Using equations (4) and (5) it can be seen that if $I = 0$ and there is only one isotope, then no incoherent scattering will occur since:

$$\overline{b^2} = \bar{b}^2$$

and therefore

$$\left(\frac{d\sigma}{d\Omega}\right)_{inc} = 0$$

The total cross-section σ_T is made up of two parts

$$\sigma_{coh} = 4\pi\bar{b}^2 \quad (17)$$

and

$$\sigma_{inc} = 4\pi(\overline{b^2} - \bar{b}^2) \quad (18)$$

Values of these cross-sections plus the absorption cross-section σ_A are shown in *Table 1* for typical nuclei found in polymers. Also included in *Table 1* are cadmium and boron which are used as neutron absorbers, vanadium which is used as a standard and aluminium and silicon which are often used in sample containers. Note that the values of $\bar{b}$

Table 1 Cross-section data for common elements

Element	I	$\bar{b} \times 10^{12}$ (cm)	σ_T (barns)	σ_{coh} (barns)	σ_A (barns)
^{1}H	1/2	−0.374	81.5	1.76	0.19
^{2}H	1	0.667	7.6	5.59	0.0005
^{12}C	0	0.665	5.51	5.56	0.003
^{14}N	1	0.94	11.4	11.1	1.1
^{16}O	0	0.580	4.24	4.23	0.0001
*Cl	3/2	0.96	15	11.58	19.5
V	7/2	−0.05	5.1	0.03	2.8
*B		0.54 + 0.021i	4.4	3.66	430
*Cd		0.37 + 0.16i	—	2.04	2650
^{27}Al	5/2	0.35	1.5	1.54	0.13
^{28}Si	0	0.42	2.2	2.22	0.06

*Naturally occurring elements which have more than one isotope

are different for ^1H and ^2H and the incoherent cross-section for ^1H is almost an order of magnitude greater than that for any other nucleus. Therefore the scattering from any sample containing hydrogen will be dominated by the hydrogen incoherent scattering.

Scattering law and correlation functions

In order to be able to use equation (9) it is necessary to reduce it to a more manageable form so that it can be related to the measured neutron spectrum. The δ function in equation (9) can be written in the form:

$$\delta(\hbar\omega + E_\lambda - E_{\lambda'}) =$$

$$\frac{1}{2\pi\hbar}\int_{-\infty}^{\infty} dt\, \exp[-it(\hbar\omega + E_\lambda - E_{\lambda'})/\hbar] \tag{19}$$

substituting this expression into equation (9) and assuming that the neutrons are unpolarized so that the average over the final and initial spin states can be dropped, the thermal average becomes:

$$\sum_{\lambda\lambda'} P_\lambda \left|\left\langle \lambda' \left| \sum_l b_l \exp(i\mathbf{Q}.\mathbf{R}_l) \right| \lambda \right\rangle\right|^2 \times$$

$$\delta(\hbar\omega + E_\lambda - E_{\lambda'})$$

$$= \frac{1}{2\pi\hbar}\int_{-\infty}^{\infty} dt \exp(-i\omega t) \sum_{\lambda\lambda'} P_\lambda \times$$

$$\left\langle \lambda \left| \sum_l b_l \exp(-i\mathbf{Q}.\mathbf{R}_l) \right| \lambda' \right\rangle$$

$$\times \left\langle \lambda' \left| \exp(itE_{\lambda'}/\hbar) \sum_{l'} b_{l'} \exp(i\mathbf{Q}.\mathbf{R}_{l'}) \times \right.\right.$$

$$\left.\left. \exp(-itE_\lambda/\hbar) \right| \lambda \right\rangle$$

$$= \frac{1}{2\pi\hbar}\int_{-\infty}^{\infty} dt \exp(-i\omega t) \sum_{\lambda\lambda'} P_\lambda \times$$

$$\left\langle \lambda \left| \sum_l b_l^* \exp(-i\mathbf{Q}.\mathbf{R}_l) \right| \lambda' \right\rangle$$

$$\times \left\langle \lambda' \left| \sum_{l'} b_{l'} \exp(itH/\hbar) \exp(i\mathbf{Q}.\mathbf{R}_{l'}) \times \right.\right.$$

$$\left.\left. \exp(-itH/\hbar) \right| \lambda \right\rangle \tag{20}$$

where H is the Hamiltonian of the array of nuclei which has eigenvalues E_λ and $E_{\lambda'}$.

Equation (20) can now be written in terms of Heisenberg time-dependent correlation functions since:

$$\exp(itH/\hbar)\exp(i\mathbf{Q}.\mathbf{R}_l)\exp(-itH/\hbar)$$

$$= \exp(i\mathbf{Q}.\hat{\mathbf{R}}_l(t)) \tag{21}$$

where $\hat{\mathbf{R}}_l(t)$ is a time-dependent Heisenberg operator. The final form of equation (9) is then:

$$\frac{d^2\sigma}{d\Omega dE} = \frac{k}{k_0}\frac{1}{2\pi\hbar}\int_{-\infty}^{\infty} dt \exp(-i\omega t) \sum_{l,l'} b_l^* b_{l'} \times$$

$$\langle \exp[-i\mathbf{Q}.\hat{\mathbf{R}}_l(0)] \rangle \exp(i\mathbf{Q}.\hat{\mathbf{R}}_{l'}(t)) \rangle \tag{22}$$

If the scattering system consists of N identical nuclei, which is a reasonable assumption if hydrogen is present as the scattering will be dominated by that from the hydrogen, then equation (22) can be written as:

$$\frac{d^2\sigma}{d\Omega dE} = \frac{k}{k_0} N\overline{b^2} S(\mathbf{Q},\omega) \tag{23}$$

where $S(\mathbf{Q},\omega)$ is called the *scattering law*[7]. $S(\mathbf{Q},\omega)$ can be divided into a coherent and an incoherent part, thus:

$$\left(\frac{d^2\sigma}{d\Omega dE}\right)_{coh} = \frac{k}{k_0} N\overline{b^2} S_{coh}(\mathbf{Q},\omega) \tag{24}$$

and

$$\left(\frac{d^2\sigma}{d\Omega dE}\right)_{inc} = \frac{k}{k_0} N(\overline{b^2} - \overline{b}^2) S_{inc}(\mathbf{Q},\omega) \tag{25}$$

where

$$S_{coh}(\mathbf{Q},\omega) = \frac{1}{2\pi\hbar N}\int_{-\infty}^{\infty} dt \exp(-i\omega t) \times$$

$$\sum_{l,l'} \langle \exp[-i\mathbf{Q}.\hat{\mathbf{R}}_l(0)] \times \exp(i\mathbf{Q}.\hat{\mathbf{R}}_{l'}(t)) \rangle \tag{26}$$

and

$$S_{inc}(\mathbf{Q},\omega) = \frac{1}{2\pi\hbar N}\int_{-\infty}^{\infty} dt \exp(-i\omega t) \times$$

$$\sum_{l} \langle \exp[-i\mathbf{Q}.\hat{\mathbf{R}}_l(0)] \exp[i\mathbf{Q}.\hat{\mathbf{R}}_l(t)] \rangle \tag{27}$$

From equations (26) and (27) it can be seen that incoherent scattering looks at correlations between the same nuclei at time zero and t whereas coherent scattering measures correlations between different nuclei.

In order to be able to relate $S(\mathbf{Q},\omega)$ to the real world, it

can be written in terms of a space–time correlation function $G(\mathbf{r}, t)$, thus:

$$S(\mathbf{Q},\omega) = \frac{1}{2\pi\hbar N} \int\int \exp(-i(\omega t - \mathbf{Q}.\mathbf{r}))G(\mathbf{r}, t)\mathrm{d}\mathbf{r}\mathrm{d}t \quad (28)$$

$S(\mathbf{Q}, \omega)$ is the double Fourier transform of $G(\mathbf{r}, t)$ where $G(\mathbf{r}, t)$ is called the *pair correlation function.* In the classical limit $G(\mathbf{r}, t)$ is the probability that if a particle is at the origin at time zero, then any particle (including the same one) will be at $\mathbf{r}$ at time t. There is an equivalent expression for $S_{\mathrm{inc}}(\mathbf{Q}, \omega)$ involving $G_s(\mathbf{r}, t)$, the *self correlation function.*

$$S_{\mathrm{inc}}(\mathbf{Q},\omega) = \frac{1}{2\pi\hbar N} \int\int \exp(-i(\omega t - \mathbf{Q}.\mathbf{r}))G_s(\mathbf{r}, t)\mathrm{d}\mathbf{r}\mathrm{d}t \quad (29)$$

where $G_s(\mathbf{r}, t)$ is the probability that if a particle is at the origin at time zero the *same particle* will be at $\mathbf{r}$ at time t.

Ideally in any neutron experiment it is necessary to measure $S(\mathbf{Q}, \omega)$ over all values of $\hbar\mathbf{Q}$ and $\hbar\omega$ in order to obtain the form of the correlation function. In practice $S(\mathbf{Q}, \omega)$ can only be measured over a limited range of $\hbar\mathbf{Q}$ and $\hbar\omega$. Normally a model correlation function is predicted and a theoretical $S(\mathbf{Q}, \omega)$ fitted to the experimental data.

One of the consequences of the correlation function formulation is that:

$$S(\mathbf{Q},\omega) = \exp(\hbar\omega/k_BT)S(-\mathbf{Q}, \omega) \quad (30)$$

The significance of this expression is that the probability of a neutron gaining energy $\hbar\omega$ is equal to $\exp(\hbar\omega/k_BT)$ times the probability that it loses energy $\hbar\omega$. Equation (30) is called the condition of detailed balance. Using equation (30) a symmetrical scattering law can be defined:

$$\tilde{S}(\mathbf{Q},\omega) = \exp(-\hbar\omega/2k_BT)S(\mathbf{Q}, \omega) \quad (31)$$

such that $\tilde{S}(\mathbf{Q}, \omega)$ is an even function in both $\mathbf{Q}$ and ω. It is $\tilde{S}(\mathbf{Q}, \omega)$ which is calculated in the inelastic experiments described below.

The scattering law separates not only into coherent and incoherent components but these are again subdivided into elastic and inelastic scattering (which includes quasi-elastic scattering). *Table 2* lists the kind of information which can be gained from these scattering experiments.

INSTRUMENTATION AND EXPERIMENTAL TECHNIQUES

Introduction

The experimental study of scattering phenomena involves the same principles irrespective of the radiation being scattered. The nature of the scattering sample influences the design of the experiment and the analysis of the data. A basic scattering experiment requires a source of radiation, some way of selecting the required energy or wavelength (monochromation) and a method of detecting the scattered radiation. Detection involves measuring the intensity as a function of momentum transfer and/or energy transfer. One can therefore divide scattering instruments into two categories, those used to measure (a) elastically and (b) inelastically scattered radiation. Instruments in category (a) are used to investigate the structural or conformational properties of a system whereas those in (b) are used to study its dynamical properties. For the purposes of this review we shall confine our remarks to instruments which have been used to study amorphous polymers.

Three basic machines will be described: in category (a) a small-angle scattering instrument which has been used very successfully to measure the conformation of polymers in the bulk and in concentrated solution; in category (b) two machines, a time of flight spectrometer which can be used to measure both quasi-elastic and inelastic spectra and a high resolution back scattering spectrometer which has been used mainly to measure quasi-elastic spectra at small values of $\hbar\mathbf{Q}$, the momentum transfer.

General considerations

Neutron source. The source of neutrons is either a nuclear reactor for a continuous beam or for a pulsed beam a *LINAC* or pulsed reactor; consequently, neutron scattering is an expensive research tool. If the information which is sought about a system can be obtained in any other way then using the alternative is highly recommended.

All the instruments described below use a reactor as the neutron source. In a typical reactor fission neutrons are produced in the core of the reactor. The energies of the neutrons are reduced by surrounding the core with D_2O which moderates the energies of the neutrons to thermal energies. A typical moderator temperature of 40°C will produce a Maxwellian distribution of neutron wavelengths peaking at about 1 Å with a long wavelength tail (*Figure 2*). The neutrons pass out of the reactor through beam tubes, the ends of which are placed near the reactor core where the peak of the thermal flux occurs.

By using a 'cold' source or a 'hot' source, it is possible to shift the wavelength distribution to produce a greater proportion of long or short wavelength neutrons, respectively. Although the peak flux near the core will be about 10^{14}–10^{15} neutrons/cm^2/sec only about 10^5–10^6 neutron/cm^2/sec will reach the sample depending on the strictness of the collimation and monochromation required for a particular experiment. Another important reason for the large drop in flux at the sample is the small amount of neutrons with a particular wavelength. It is clear from *Figure 2* that relative to the peak λ there are very few neutrons with a long wavelength. Using a 'cold' source can increase the flux at longer wavelengths by up to a factor of 8 but this still means the flux is very low.

Monochromation. Monochromation of a neutron beam can be achieved in a number of ways. Two basic methods are used. The first method involves the use of a crystal which will scatter particular wavelength neutrons if placed at the correct angle to the incoming beam in accordance

Table 2

Type of scattering	Information obtained from polymers
Coherent:	
Elastic	Crystal structure, conformation of chains in the bulk and in solution
Inelastic	Phonon dispersion curves
Quasi-elastic	Dynamics of polymer chains
Incoherent:	
Elastic	
Inelastic	Molecular spectroscopy, vibrational spectra of polymer side chains
Quasi-elastic	Dynamics of polymer chains

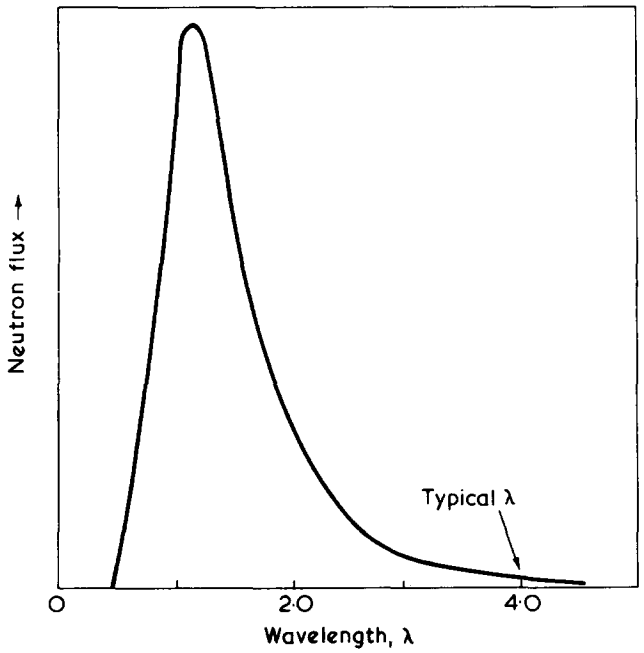

Figure 2 The distribution of neutron flux as a function of wavelength for a moderator temperature of 40°C. λ_{max} = 1.1 Å

with Bragg's Law. Crystals can also be used as filters which only allow neutrons with wavelengths greater than the Bragg cut-off to pass through, e.g. Be has a Bragg cut-off of 3.96 Å so that only long wavelength neutrons can pass through the crystal, all others being reflected.

The second method of monochromation involves the use of mechanical velocity selectors which come in two main types. A continuous beam of neutrons with a particular wavelength distribution can be produced by using a helical velocity selector. *Figure 3a* shows a diagrammatic representation of a helical velocity selector. This type of selector has helical slots cut along the length of the cylinder parallel to the axis of rotation. The wavelength of the neutrons selected can be varied by varying the speed of rotation of the selector. The width of the wavelength distribution can be altered by changing the number and size of the slots and also by changing the length of the selector.

The second type of mechanical selector produces pulses of neutrons. *Figure 3b* shows a typical rotor or chopper. The rotor consists of a Mg–Cd alloy block into which a number of curved slots have been cut. When rotated with the axis of rotation perpendicular to the incoming beam the rotor will only allow through pulses of neutrons with energies within a narrow distribution. This distribution is determined by the speed of rotation of the rotor and the number and width of the slots. To obtain better energy resolution it is common practice to use two such rotors which are phased relative to one another to produce a narrow pulse. The factors affecting the resolution of these rotors have been discussed by Harriman and Hayter[8]. An important point to remember is that, normally associated with any improvement in energy resolution is a decrease in flux.

Neutron detection. Thermal neutrons are counted by detecting the recoil products of their reaction with certain nuclei, in particular ^{10}B, ^{3}He or ^{6}Li. The products of these reactions can then be detected either by ionization of a gas, or by light emission (in scintillation counters). Detectors commonly contain $^{10}BF_3$ or ^{3}He gas at a pressure of a few atmospheres in a cylindrical tube about 2 to 5 cm in diameter and up to 50 cm long. Depending upon whether spatial or time resolution is required, these detectors can be used end-on or side-on.

The detection efficiency of a gas counter approaches 100% although the efficiency of the detector varies with the energy of the incident neutrons. Corrections therefore have to be made for this effect on any neutron spectra.

Recently position-sensitive BF_3 detectors have been developed which consist of grids of horizontal and vertical electrodes making a number of cells. A neutron is detected by a signal from one vertical and one horizontal electrode thus giving its position on the detector. One such detector is in use on the small-angle instrument at Grenoble and has a grid of 64 x 64 electrodes giving 4096 cells, each 1 cm^2.

On most instruments it is necessary to monitor the intensity of the incident beam and for this process uranium fission counters are used. This type of counter has a low cross-section, so that most of the beam is transmitted, but has very high counting efficiencies. Another advantage is that they are very thin so that their spatial resolution is very much better than the normal gas counters.

Sample considerations

The size and thickness of the sample to be studied as well as the material used for containment depends on the scattering experiment. The thickness of the sample is related to the cross-section, σ, by the Beer–Lambert law:

$$I = I_0 \exp(-n\sigma L) \qquad (32)$$

where I_0 is the incident flux, I is the transmitted flux, n is the number of atoms per unit area and L is the thickness of the sample. For an inelastic or quasi-elastic experiment the thickness of the sample is chosen so that it will scatter about 10% of the beam. The figure of 10% is chosen in order to minimize multiple scattering effects. In a small-angle experiment samples are normally much thicker and up to 50% of the beam is scattered.

Values of L for hydrogenous and deuterated polystyrene are listed in *Table 3* for both a 10 and 50% scatterer.

The size of the sample depends on the beam area. For a typical inelastic experiment the sample will be 25 cm^2 whereas for a small-angle experiment it will be 1 cm^2.

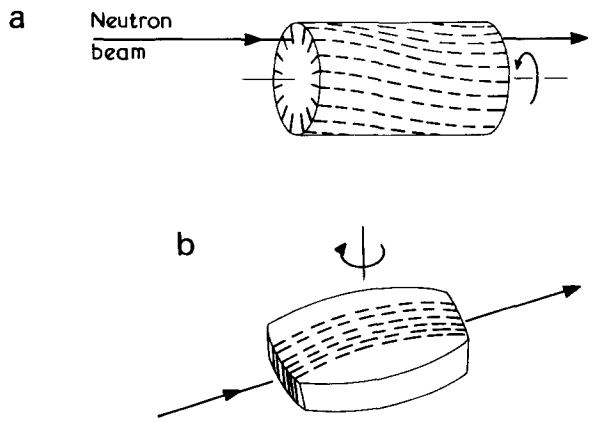

Figure 3 Diagram of two types of mechanical monochromators: (a) a helical slot velocity selector and (b) a 6 slot Harwell rotor

Table 3

Polymer	σT (barns)	n $\times 10^{-23}$	L_1 (cm) ($I/I_0 = 0.9$)	L_2 (cm) ($I/I_0 = 0.5$)
Polystyrene	696.08	0.058	0.025	0.17
Deuterated polystyrene	104.88	0.054	0.18	1.2

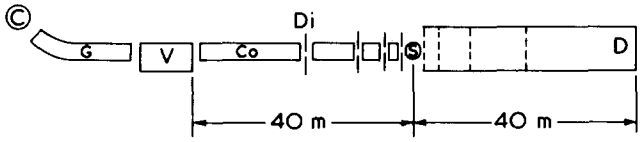

Figure 4 Diagram of the small-angle diffractometer D11 at the ILL, Grenoble

The material used to contain the sample also depends on the experiment. In an inelastic experiment aluminium or aluminium–magnesium alloy containers are normally used. But aluminium is not normally used for small-angle experiments as it gives a small angle signal at low Q thus making background subtraction difficult, instead, silica cells are used.

It is also necessary to ensure that the neutron beam only scatters off the sample, to do this cadmium or gadolinium masks are used to absorb any stray neutrons.

NEUTRON SCATTERING INSTRUMENTS

Elastic scattering

Small-angle scattering diffractometer, instrument description. In small-angle neutron scattering (SANS) the intensity of the scattered beam is measured as a function of the angle of scatter in the range $\theta = 50°$ to $0.15°$; no energy analysis is carried out. *Figure 4* shows a schematic diagram of D11[9] at the Institut Laue–Langevin (ILL), Grenoble. A liquid $^2H_2$ 'cold' source, C, produces long wavelength neutrons which then pass through a curved guide, G. The guide reduces the amount of γ rays and fast neutrons in the beam. The required wavelength, in the range 5 to 12 Å, and wavelength distribution are determined by a helical slot velocity selector, V. Two velocity selectors are available with different resolutions.

After the selector, the beam is collimated using diaphragms, Di, and neutron guides, Co, which can be moved out of the beam so as to produce the apparent neutron source at different distances from the sample. The apparent source can be placed at 5 positions between 2 and 40 m from the sample.

On the other side of the sample, S, there is a large evacuated tube into which the position sensitive detector, D, can be placed at 5 points from 2 to 40 m from the sample. In this way it is possible to change the range of Q which can be covered by varying the distance between the sample and the detector. *Figure 5* shows the range of Q which can be covered at each detector position using wavelengths of 5 and 12 Å.

The detector consists of a matrix of 64 x 64 1 cm^2 cells (4096 cells). The data from the detector is collected by a PDP11 computer and is displayed on a visual display unit.

Experimental considerations. The size of the sample required and sample containment, where necessary, have been described above. If single particle behaviour is to be measured then the concentration of tagged molecules must be low so that no interparticle interference effects occur.

The length of a measurement can vary from 5 min to 8 h or longer, depending on a number of factors. As the detector is moved further away from the sample then the solid angle it subtends decreases and therefore so does the number of detected scattered neutrons. As the apparent source is moved further from the sample the incident flux decreases so that the time for a measurement increases. The time for a measurement is also affected by the number of scattering centres and the contrast factor (see below).

Another important factor affecting the length of the experiment is whether or not the scattering from the sample is isotropic. Measurement of a normal isotropic pattern will take between 5 min and 1 h. In this case the data is analysed by averaging the counts in the detector as a function of r, the distance from the centre (*Figure 6a*).

If the sample is anisotropic, e.g. a stretched or oriented polymer then it is necessary to analyse the scattering in different directions and thus not all the data are used. Usually only small segments of the detector are analysed. This is illustrated in *Figure 6b* where segments in different directions are indicated The number of counts per cell has therefore to be much greater than for an isotropic experiment in which the intensity as $f(r)$ is averaged over many cells; hence the experiment takes longer.

Although the contrast factor is the same, if one uses a hydrogenous matrix with a small amount of deuterated polymer or *vice versa*, there are problems due to void scattering which can be minimized if a hydrogenous matrix is used. On the other hand a hydrogenous matrix gives rise to a highly incoherent background.

The detector response for different cells is not always uniform. To measure this it is necessary to measure the

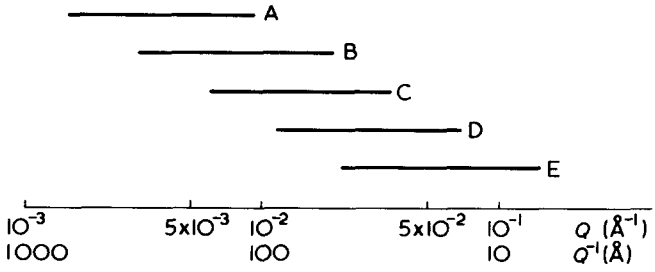

Figure 5 The Q ranges covered on D11 at different distances of the detector from the sample. A, 40 m; B, 20 m; C, 10 m; D, 5 m; E, 2 m

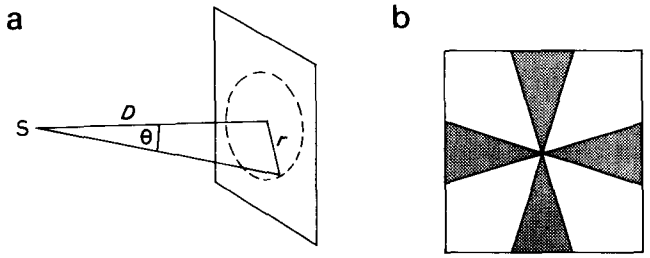

Figure 6 Analysis of SANS data. (a) In an isotropic experiment the intensity I as $f(r)$ is averaged over the whole detector whereas (b) for anisotropic scattering, segments of the detector are analysed. $Q = 2\pi r/\lambda D$

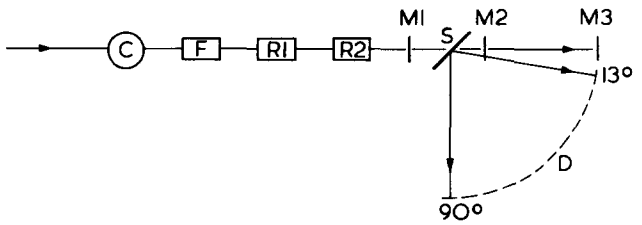

Figure 7 Diagram of the time of flight spectrometer 4H5 at AERE, Harwell

scattering from a standard which has a flat signal over the Q range being used. Any variation in the signal is a measure of the detector response.

The length of time required to carry out a series of experiments must take into account the amount of time to change a sample (usually minimal) and to change the position of the detector (~4 h) if a different Q range is required. If temperature variation is to be carried out this will also take time (~½ h) for each interval.

Data analysis. Measurements of the radius of gyration, R_g, of a polymer are made on a solution of a few percent of tagged polymer in a matrix (solid or otherwise) and on a background sample which will be the polymer matrix (solid solution) or solvent (normal solution). The background sample must also take account of the excess incoherent scattering from the tagged polymer so that if the tagged polymer is hydrogenous then an equal amount of hydrogen in the form of small molecules must be dispersed in the deuterated background. The same holds for a deuterated sample but in this case the amount of incoherent scattering from a small amount of deuterium in a large amount of hydrogen is usually negligible.

Account must also be taken of differences in the run times or monitor counts, the efficiency of the detector, differences in the transmissions of the sample and background and if molecular weights are to be measured then a standard scatterer must be used to normalize the data. Data analysis is essentially the same as that used for conventional light scattering.

The data is first of all averaged over different values of r, the radius from the centre of the detector, to give the intensity I as $f(r)$. Usable values of r are from 7 to 32 cm. The background scattering is then subtracted and any corrections made to the data. Q is calculated knowing the distance of the sample from the detector D, and the incident wavelength, λ, using the expression

$$Q = \frac{2\pi}{\lambda}\frac{r}{D} \qquad (33)$$

The data in the form I as $f(Q)$ can then be manipulated in the appropriate way.

Inelastic scattering

Time of flight spectrometer, instrument description. The basic principle of a time-of-flight (*TOF*) spectrometer is that by measuring the time a neutron takes to travel a known distance one can calculate its velocity and hence its energy. *TOF* spectrometers are used to measure inelastic and quasi-elastic spectra. *Figure 7* shows a diagrammatic representation of a typical *TOF* spectrometer 4H5[10] at AERE, Harwell, UK.

Neutrons pass through a liquid H_2 'cold' source, C, followed by Be and Bi crystals, F, which reduce the γ ray and fast neutron components. The Be crystal also acts as a filter. The beam is then monochromated using twin rotors, R1 and R2, which also pulse the beam. Pulses arriving at the sample, S, are scattered and the scattered neutrons are detected by banks of BF_3 detectors, D, at 13 fixed angles of scatter between 13° and 90° to the incident beam. Monitors M1, M2 and M3 are fission counters at known distances from the sample position which are used to calculate the energy of the incident neutrons and also the transmission of the samples. The flight path between the sample and detectors varies from 1.2 to 1.9 m.

Neutrons arriving at different times at a particular detector or monitor are sorted into time channels, normally 6 or 8 μs wide, the total number depending on the rotor period and the channel width; a maximum number of 512 channels is available. A typical spectrum from a polymer is shown in *Figure 8* for the 72° detector. The data are collected on a PDP-8 on-line computer.

Experimental considerations. It is usually necessary either to evacuate the sample chamber or fill it with helium to eliminate air scattering close to the sample. On 4H5, the sample changer has three positions which are placed in the beam in rotation. The three positions usually hold a sample, empty container and vanadium. The vanadium is used to measure the resolution of the machine and to correct for the efficiencies of the different detectors. A normal experiment on a polymer (10% scatterer), container and vanadium will take 24 h but it is often necessary to use much longer times to obtain good inelastic spectra.

The resolution of the machine and the incident flux should be optimized for each experiment. On 4H5, using two 6 slot rotors an incident energy of 3.5 meV will have a resolution (full width at half maximum, *FWHM*, of the vanadium elastic peak) which varies with angle of scatter from 0.35 to 0.43 meV. If two 12 slot rotors are used the resolution then becomes 0.15 to 0.25 meV, but the flux drops by a factor of 3.

Higher resolution and increased flux have been achieved on the multichopper *TOF* spectrometer IN5[11] at the ILL, Grenoble. For an incident energy of 0.8 meV the resolution is about 25 μeV.

The Q range on 4H5 is between 0.5 and 2 $Å^{-1}$. Smaller Q values can be achieved on IN5 down to 0.1 $Å^{-1}$.

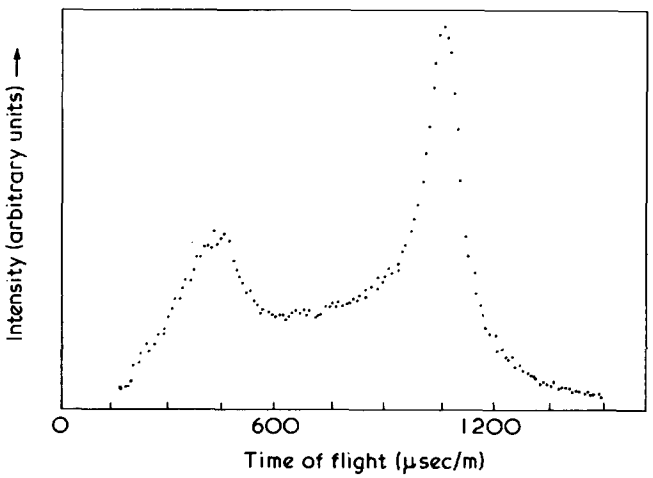

Figure 8 A typical *TOF* spectrum from an amorphous polymer. The spectrum was obtained using 4H5 with two 6 slot rotors at a scattering angle of 72° from poly(dimethyl siloxane) at 20°C

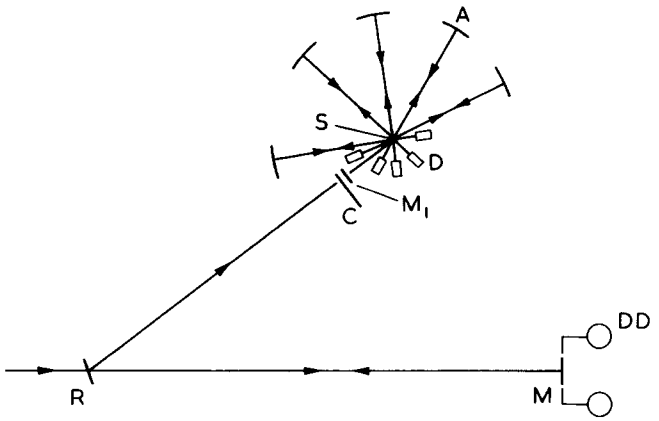

Figure 9 Diagram of the back-scattering spectrometer INIO at ILL, Grenoble

Because of the low incident energies of both 4H5 and IN5 only neutron energy gain spectra can be measured.

Data analysis. *TOF* spectrometers measure the intensity of the scattered beam as a function of time of flight and angle of scatter. The scattering from the container is first subtracted from the sample plus container scattering and corrections are made for: (1) differences in the length of time that the sample and background were in the beam; (2) the efficiency of the detectors, and (3) differences in path length of the sample and vanadium as the angle of scatter changes. Other corrections can also be made, e.g. if there is a flat background due to radiation from another source this must be subtracted.

The count rate, C, from the sample is related to the double differential cross-section $d^2\sigma/d\Omega d\tau'$ by the expression:

$$C = nN \frac{d^2\sigma}{d\Omega d\tau'} \Delta\Omega \Delta\tau \epsilon_{\tau'} \tag{34}$$

where N is the number of incident neutrons, n is the number of atoms/cm^2 in the sample, $\Delta\Omega$ is the solid angle subtended by the detector at the sample, $\Delta\tau$ is the channel width and $\epsilon_{\tau'}$ is the efficiency of the detector to neutrons of time of flight τ'.

The double differential cross-section is then related to the scattering law by the expression:

$$S(\mathbf{Q},\omega) = \frac{d^2\sigma}{d\Omega d\tau'} \frac{\tau'^4}{\tau_0} \frac{\hbar}{m} \frac{4\pi}{\sigma} \tag{35}$$

Because of the factor τ'^4/τ_0 the *TOF* spectra are considerably altered when the final $S(\mathbf{Q},\omega)$ is calculated.

Having calculated $S(\mathbf{Q},\omega)$ further analysis can then be carried out on the spectra to obtain, e.g. the torsional frequency of a CH_3 group from the inelastic spectrum or information about the diffusional motions of the polymer chain from the quasi-elastic scattering.

High resolution back-scattering spectrometer, instrument description

A diagrammatic picture of the back-scattering spectrometer[12], INIO, at the ILL, Grenoble is shown in *Figure 9.*

The neutron beam is Bragg-reflected at 90° by the monochromator, M, it is then reflected by the crystal, R, onto the sample, S. The scattered neutrons are again Bragg reflected at 90° by the analyser crystals, A, into the detectors, D. Up to 5 sets of analysers and detectors can be used to cover scattering angles between −10° and 160°. The box containing the sample and detectors is filled with He. In order to be able to investigate inelastic events, the energy of the incident neutrons is varied by Doppler motion of the monochromator crystal in the direction of the beam. By changing the monochromator crystal or the Doppler velocity different energy windows can be produced. The resolution of INIO is very good (~1μeV) with a Q range depending on the crystals used of 0.1 to 4 Å^{-1}. The energy window produced by Doppler shifting the monochromator varies from ±6 to ±12 μeV using the Si(111) plane. INIO is therefore used for low Q measurements where the energy changes are very small. Quasi-elastic scattering and tunnelling phenomena have been measured using INIO. The data is collected by a PDP-11 on-line computer.

Experimental considerations. The beam size on INIO is 3 x 3 cm^2 so that the maximum sample size is smaller than that of the *TOF* spectrometers. Because of the geometry of the machine it is necessary to have sample containers which are as thin as possible. Measurements are made on a sample, container and vanadium as in a *TOF* experiment.

Data analysis. The raw data which is collected as counts as a function of energy transfer for the different detectors is first of all normalized by the monitors. The analysis of the data essentially proceeds then as for the *TOF* analysis except that $d^2\sigma/d\Omega dE$ is measured not $d^2\sigma/d\Omega d\tau$. Therefore:

$$S(\mathbf{Q},\omega) = \frac{d^2\sigma}{d\Omega dE} \frac{k}{k_0} \hbar \frac{4\pi}{\sigma} \tag{36}$$

where k and k_0 are the final and initial scattering vectors.

CONFORMATION STUDIES OF POLYMERS BY NEUTRON SCATTERING

Introduction

In this section we discuss the theory of small-angle neutron scattering (SANS) with respect to the determination of structural parameters. Amorphous systems only are considered but studies of crystalline polymers are reported in the literature.

Even with this limitation the applications of SANS are manifold and new regions of application are still being exploited. We review the major advances made by the technique and discuss some of the latest results.

Theory

For a system of N nuclei, the intensity of neutrons scattered through an angle $d\Omega$ with an energy change dE is, from equations (24) and (25):

$$\frac{d^2\sigma}{d\Omega dE} = \frac{k}{k_0} |b^2_{coh} S_{coh}(\mathbf{Q},\omega) + b^2_{inc} S_{inc}(\mathbf{Q},\omega)| \tag{37}$$

where $b^2_{coh} = \overline{b}^2$ (see discussion on scattering length); $b^2_{inc} = \overline{b^2} - \overline{b}^2$, an experimentally undeterminable quantity [but $\sigma_{inc} = 4\pi(\overline{b^2} - \overline{b}^2)$]; b^2_{inc} is used here as an expedient to simplify the equations appearance.

For small-angle neutron scattering we are only interested in *elastic* scattering processes, i.e. $dE = 0$ and $k = k_0$. Furthermore only the coherent scattering retains the inter-

ference effects characteristic of the structure of the scattering materials. The incoherent scattering is isotropic and provides a background on which the coherent scattering is superimposed. If the scattering substance is a mixture of N_1 molecules of substance 1 dissolved in N_2 molecules of substance 2, then we may rewrite equation (37) as[5]:

$$\frac{d\sigma}{d\Omega} = (b_{1coh} - b_{2coh}\bar{V}_1/\bar{V}_2)^2 S_{1coh}(Q) + N_1 b_{1inc}^2 + N_2 b_{2inc}^2 \quad (38)$$

where b_{icoh} is the sum of the nuclear coherent scattering lengths in the molecule and b_{iinc} is the sum of the nuclear 'incoherent scattering lengths' in the molecule. $\bar{V}_1$ and $\bar{V}_2$ are the partial molar volumes of substances 1 and 2, respectively.

If we are able to subtract from equation (38) the incoherent background scattering, then the excess scattering $(d\sigma/d\Omega)_{Ex}$ contains all the information about the structure of the scattering material since:

$$\left(\frac{d\sigma}{d\Omega}\right)_{Ex} = (b_{1coh} - b_{2coh}\bar{V}_1/\bar{V}_2)^2 S_{1coh}(Q) \quad (39)$$

$S_{1coh}(Q)$ is the Fourier transform of the density fluctuation correlation function of the scattering centres, and[13]:

$$S_{1coh}(Q) = \sum_{ij} \langle [\exp i\mathbf{Q}.(\mathbf{r}_i - \mathbf{r}_j)]^2 \rangle$$

where $\mathbf{r}_i$ and $\mathbf{r}_j$ are the centres of mass of the scattering points i and j. For a polymer molecule the scattering points are the chain segments. In terms of polymer chain dimensions the coherent scattering law can be written as:

$$S_{1coh}(Q) = N_1^2 2/(Q^2\langle s^2\rangle)^2 \times [\exp(-Q^2\langle s^2\rangle) - 1 + Q^2\langle s^2\rangle]$$

where N_1 is the number of segments in a chain whose mean square radius of gyration is $\langle s^2\rangle$.

Thus replacing in equation (39):

$$\left(\frac{d\sigma}{d\Omega}\right)_{Ex} = (b_{1coh} - b_{2coh}\bar{V}_1/\bar{V}_2)^2 N_1 2/(Q^2\langle s^2\rangle)^2 \times [\exp(-Q^2\langle s^2\rangle) - 1 + Q^2\langle s^2\rangle]$$

$(b_{1coh} - b_{2coh}\bar{V}_1/\bar{V}_2)^2$ is the contrast factor K, and clearly the larger this value, the more intense the scattering.

For a polymer of molecular weight M and concentration c(wt/vol) then the intensity of scattering per unit volume, $I(Q)$ is:

$$I(Q) = \left(\frac{d\sigma}{d\Omega}\right)_{Ex} \frac{c}{M} N_A = \frac{Kc}{M} N_A N_1^2 2/(Q^2\langle s^2\rangle)^2 \times [\exp(-Q^2\langle s^2\rangle) - 1 + Q^2\langle s^2\rangle]$$

with N_A = Avogadro's number.

Since $N_1 = M/m$, where m is the molecular weight of a segment unit, then:

$$\frac{KcN_A}{M} N_1^2 = \frac{KcN_A}{M}\frac{M^2}{m^2} = K^*cM$$

with

$$K^* = KN_A/m^2$$

giving:

$$I(Q) = K^*cM2/(Q^2\langle s^2\rangle)^2 [\exp(-Q^2\langle s^2\rangle) - 1 + Q^2\langle s^2\rangle]$$

Therefore:

$$K^*c/I(Q) = M^{-1}\{2/(Q^2\langle s^2\rangle)^2 \times [\exp(-Q^2\langle s^2\rangle) - 1 + Q^2\langle s^2\rangle]\}^{-1} \quad (40)$$

Depending on the value of Q *vis-à-vis* the molecular parameters of the polymer chain, we can discern four regions of distinct scattering behaviour from equation (40)[14].

(A) $Q < \langle s^2\rangle^{-1/2}$ the Guinier range; equation (39) reduces to:

$$K^*c/I(Q) = M^{-1}(1 + Q^2\langle s^2\rangle/3) \quad (41)$$

From which the molecular weight and radius of gyration are easily obtainable.

(B) $\langle s^2\rangle^{-1/2} \leqslant Q \leqslant a^{-1}$ where a is the persistence length of the polymer chain. Scattered intensity approaches an asymptotic value described by:

$$K^*c/I(Q) = M^{-1}Q^2\langle s^2\rangle/2 \quad (42)$$

(C) $a^{-1} < Q < l^{-1}$ where l = statistical step length of the polymer. The scattered intensity is characteristic of a rod of length nl where n is the number of statistical units in the chain:

$$K^*c/I(Q) = M^{-1}nlQ/\pi \quad (43)$$

(D) $l^{-1} < Q$, has a scattered intensity governed by the structure of the segments forming the chain. No asymptotic expression is yet available for this region.

In principle these regions can be distinguished from each other by using the well known Kratky plot, an idealized form of which is shown in *Figure 10*.

The similarity of equation (41) to the light scattering equation will have been noted. As in light scattering, thermodynamically non-ideal environments can be encompassed by rewriting equation (41) in the familiar Zimm form[15]:

$$K^*c/I(Q) = M^{-1}(1 + Q^2\langle s^2\rangle/3) + 2A_2c + 3A_3c^2 \quad (44)$$

By extrapolating a series of measurements at different c and Q (≡ angle in light scattering) to $c = 0$ and $Q = 0$ we can obtain $\langle s^2\rangle$ and M. For polydisperse polymers the values are $\langle s^2\rangle_z$ and $\bar{M}_w$, respectively.

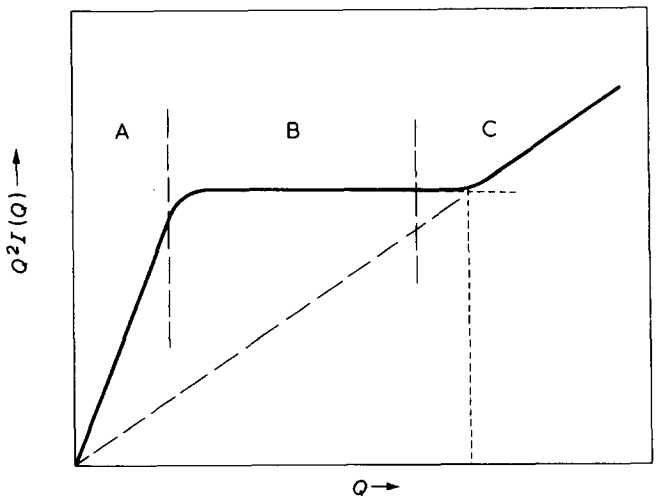

Figure 10 An idealized Kratky plot showing regions A to C explained in the text

Table 4 Contrast factors for neutron (K) and X-ray scattering (K_X) for polymer–diluent systems

Polymer	Solvent	$10^{28}K$ (m^2)	$10^{28}K_X$
Hydrogenous polystyrene	Benzene, C_6H_6	0.13	6.3
	Benzene, C_6D_6	73.70	2.3
	Cyclohexane, C_6H_{12}	8.1	11.75
	Deuterated polystyrene	70.2	0
D–PMMA	H–PMMA	70.2	0

Contrast factor

The equations developed above are equally applicable to X-ray and light scattering. Neutrons are particularly powerful in examining the structure and dynamics (see below) because the scattering vector is reasonably large and neutron energy is reasonably low. For neutrons $Q \sim 1$ Å^{-1}, energy ~0.1 kJ/mol whilst for visible light $Q \sim 10^{-3}$ Å^{-1}, energy ~200 kJ/mol. The extremely small Q of visible light confines light scattering to the Guinier range, and modern instrument developments using laser sources produce even smaller values of Q[16].

Small-angle X-ray scattering on the other hand has the same range in scattering vector as neutron scattering. The extremely rapid development of SANS in preference to small-angle X-ray scattering is due to the much larger contrasts available in neutron scattering. Due to the difference in coherent scattering lengths (see *Table 1*) between hydrogen and deuterium, a sizeable contrast (and hence measurable scattering) can be generated by dispersing a small concentration of fully deuterated polymer in a hydrogenous matrix or *vice versa*.

Contrast factors for some typical polymer–diluent systems are given in *Table 4* together with X-ray contrasts calculated from the formula of Kirste and Wunderlich[17]. Clearly deuteration offers much greater scope in neutron scattering, especially where one polymer is dissolved in another, enabling dimensions in the bulk state to be obtained. Although improvements in X-ray scattering can be obtained by heavy atom labelling, this drastically alters the chemical integrity of the polymer molecule thus introducing other problems. (We note that recent publications in small-angle X-ray scattering seem to have overcome this and other problems[18,19]). In contrast deuteration does not markedly influence the thermodynamic properties of the polymer, though there are detectable differences in some polymer systems.

Experimental results

An exhaustive review of all the results so far published would be far too large for our present purposes. Such reviews are available elsewhere[20,21]. Results which have had a major impact on polymer science will be reviewed here, although plentiful references will be given to similar experiments on different systems.

Bulk polymers. Undoubtedly the most dramatic proof of the power of SANS came in this field. On semiempirical grounds, Flory[22] proposed some thirty years ago that amorphous polymers in their bulk state should have unperturbed dimensions and an interpenetrable Gaussian coil structure.

Cotton *et al.*[23] carried out a thorough investigation of bulk amorphous polystyrene although similar types of results had been published a little earlier[24–27]. The type of scattering pattern obtained by Cotton *et al.* from a bulk polystyrene (PSH) 'doped' with deuterated polystyrene (PSD) is shown in *Figure 11*. Results were also obtained for solutions of the polymer in carbon disulphide and in a θ solvent. These results are given in *Table 5*, together with values expected from the more usual (e.g. light scattering) dilute θ solution studies.

For the bulk polymers, Zimm diagrams showed that $A_2 \simeq 0$ indicating that the interaction between deuterated and hydrogenated polymer is undetectably different from the interaction between hydrogenated polymer chains. Furthermore the results followed the form of the Debye

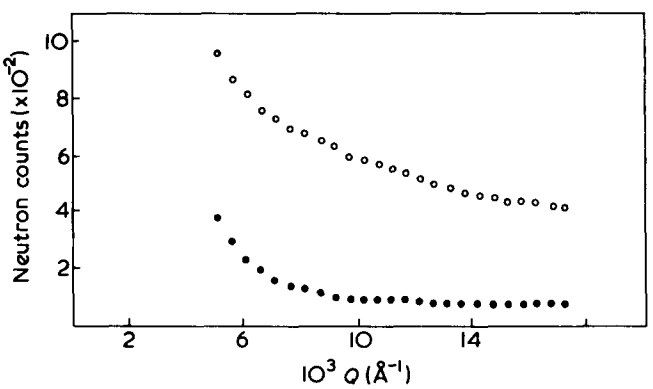

Figure 11 Small-angle scattering obtained from: ●, PSH and ○, PSH plus 2% PSD ($M_W = 1.4 \times 10^5$)

Table 5 Weight-average root mean square radii of gyration for polystyrene in differing environments determined by SANS[21]

$10^{-5}M_W$	CS_2	C_6H_{12}(36°)	Bulk	Literature value
0.21	5.0	4.2	3.8	3.96
0.57	8.4	7.0	5.9	6.53
0.90	11.5	8.8	7.8	8.2
1.12	–	–	8.7	9.15
1.60	16.8	11.7	10.7	10.9
3.25	20.4	15.0	14.3	15.6
5.00	–	19.1	21.3	19.3
11.00	56.8	29.3	29.7	28.7

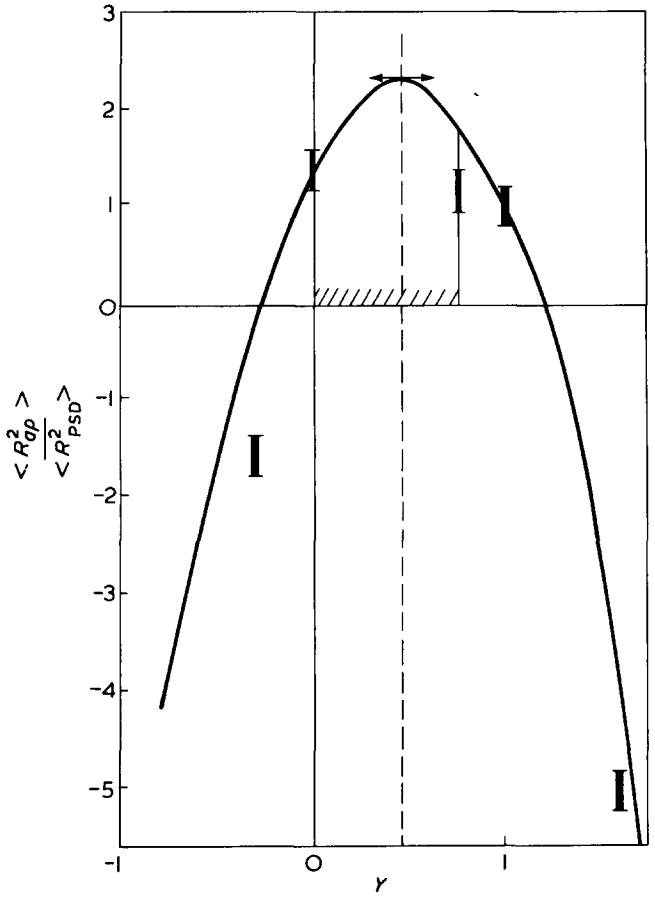

Figure 12 Plot of $\langle R^2_{ap}\rangle/\langle R^2_{PSD}\rangle$ against Y, the contrast between block 1 (PSD), block 2 (PSH) and the solvent (a mixture of C_6D_{12} and C_6H_{12}). The curve is calculated from theory [Reproduced from Duval, M., Duplessix, R., Picot, C., Decker, D., Rempp, P., Benoit, H., Cotton, J. P., Jannink, G., Farnoux, B. and Ober, R. *J. Polym. Sci (Polym. Lett. Edn)* 1976, **14**, 585 by permission of John Wiley and Sons, Inc. ©]

equation for a Gaussian coil. Strictly speaking, the condition of $A_2 \simeq 0$ is only true for cases where solute (deuterated polymer) and solvent (hydrogenated polymer) have infinite molecular weight and are chemically identical. The influence of the molecular weight of the solvent on A_2 has been admirably demonstrated by the work of Kirste *et al.* on solutions of PDMS in oligomeric deuterated siloxanes[28].

Although Pechhold[29] has derived scattering laws from the meander model which also follows the Debye curve, the weight of evidence (see below) supports Flory's theory. Results from poly(ethylene oxide)[30], poly(dimethyl siloxane)[24], poly(vinyl chloride)[31] and polyethylene[32] all show the same behaviour (in the amorphous state) as polystyrene, i.e. unperturbed dimensions and Debye-type scattering curves. Polyethylene presented some initial practical difficulties due to clustering of deuterated species in the matrix, but these were subsequently overcome by use of a different solvent in the preparation of the mixtures.

Preliminary results of compatibility studies in bulk polymers have been published by Kirste *et al.*[33] and Ballard and coworkers[34]. Allen and colleagues[35] have examined the change in polystyrene dimensions in a polystyrene–polybutadiene mixture as the mixtures were cooled through the phase separation curve. Preliminary analysis of the results shows that the polystyrene has smaller dimensions at temperatures below the phase transition temperature.

Studies on poly(methyl methacrylate) by Kirste and coworkers[36] duplicated earlier small-angle X-ray scattering in θ solvents. The dimensions of the molecules were unperturbed, but the scattering pattern showed no plateau in the intermediate Q region ($\langle s^2\rangle^{-1/2} \leqslant Q \leqslant a^{-1}$), a marked decrease in intensity being observed. Flory and Yoon[37,38] reproduced this scattering curve almost exactly using rotational isomeric state theory for a random coil structure. SANS has thus provided a good example of the power of rotational isomeric state theory as well as proving the existence of unperturbed random coils in solution.

Dilute solution studies. There is little advantage of SANS over that of light scattering for classical dilute solution studies. However Ballard and coworkers[39] used the wider range of scattering vector available to measure dimensions of very low molecular weight polystyrenes (4×10^3 to 6×10^2). In this region of molecular weight the Kratky–Porod worm-like chain fitted the results best. Persistence lengths of cellulose tricarbanilate[40] and polyelectrolytes[41] have been obtained by the technique. Furthermore, neutron scattering from semi-dilute polyelectrolyte solutions revealed a Bragg-like peak indicative of some form of ordering in the solution[42]. This ordering is predicted by the cell theory of Katchalsky[43] and the recent correlation length theory of De Gennes *et al.*[44].

It has been known for a number of years that copolymer dimensions are grossly affected by the solvent in which they are measured[45]. This effect of course is due, in part, to thermodynamic influences, but more particularly it arises from the arrangement of the chemically different units in the copolymer influencing the angular distribution of the scattered radiation and the contrast factors. Together these lead to apparent values for the dimensions being obtained. True values can be obtained only from a series of measurements in solvents with different contrasts. Unfortunately, changing solvents changes the polymer dimensions via thermodynamic effects, and consistent results in this field are rare. However, Duval *et al.*[46] have used mixtures of deuterated and hydrogenated cyclohexane to obtain solvents of differing contrast but similar thermodynamic properties. By this means the change in dimensions of a PSD–PSH block copolymer with contrast were almost exactly as predicted by theory (see *Figure 12*). SANS was used in conjunction with classical light scattering to determine the structure of a polystyrene–poly(methyl methacrylate) copolymer by Han and Mozer[47]. Finally in this section we mention some results of experiments made on linear and cyclic poly(dimethyl siloxanes)[48]. Theoretical treatments[49] for infinite molecular weight polymers suggest that, for the same molecular weight, linear chain dimensions should be twice that of the cyclic chains. Additionally, $S(Q)^{-1}$ for cyclic polymers should curve upwards. Experimental $S(Q)^{-1}$ were indeed this shape; however, linear chains were only 1.5 times as large as rings of the same molecular weight. This discrepancy may be attributable to either chain expansions due to working in good solvents or the difficulty in determining the limiting slope at $Q = 0$ from the scattering envelope of the cyclic polymers.

Stretched polymers. Clearly SANS will be of great value in testing the assumptions on which the molecular theory of rubber elasticity is based. Chief amongst these is the principle of affine deformation. Benoit *et al.*[50] have proposed an 'end-to-end pulling' mechanism for chain extension whereby the middle of the chain is less extended than the ends. Neutron scattering experiments on quenched, hot stretched uncrosslinked polystyrenes did not support

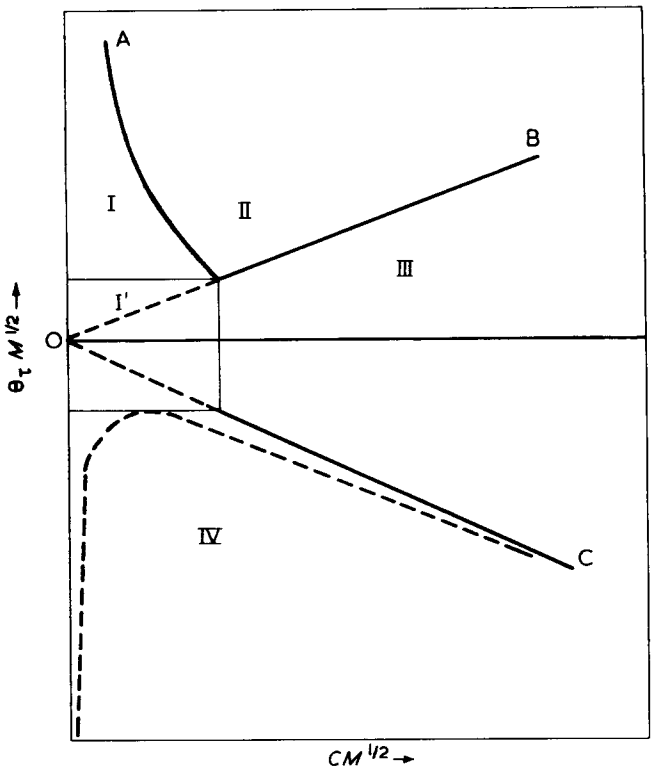

Figure 13 The temperature – concentration diagram derived from renormalization group theory of polymer solutions. The different regions are explained in the text A, C^*; B, C^{**}; C, $-C^{**}$

this model[51]. However, neither did they support the affine deformation principle, the dimensions being somewhat less than calculated by this model. This disagreement could possibly be due to relaxation of the chains during quenching. Additionally results presented by Boué[52] support the 'end-to-end pulling' model. Chain dimensions of stretched polystyrenes determined at low Q behaved affinely. From scattering at intermediate $Q(\langle s^2\rangle^{-1/2} \leqslant Q \leqslant a^{-1})$, dimensions within $\langle s^2\rangle$ showed no such affine behaviour.

The process of stress relaxation at elevated temperatures in a stretched polystyrene has been examined by SANS[53]. Preliminary results agree qualitatively with mechanical measurements by showing a rapid decrease of dimensions in the early stages of relaxation with a long 'tail' at longer relaxation times. SANS results have also been obtained for stretched polybutadiene containing deuterated polybutadiene[54]. The results were somewhat inconclusive, undoubtedly the low signal intensity from the system (K = 39×10^{-28} m^2) is an important factor in this uncertainty.

Concentrated solutions. The advent of small-angle neutron scattering has been of great impetus to the study of solutions with concentrations outside the usual dilute maximum of 1% wt/vol. By doping the solute with a low concentration of deuterated polymer, the scattering centres themselves are still in the dilute regime, being well separated from each other, but are subject to all the thermodynamic influences present in a concentrated solution.

Theory of such solutions has been developed via an analytical mean field approach and a renormalization group-scaling law approach. To review the two approaches is beyond the scope of the present article and the interested reader can consult the original papers in conjunction with an introduction to renormalization group theory[55–61]. A brief summary of the underlying philosophy common to both approaches is all that is given here.

In a dilute polymer solution, intramolecular excluded volume interactions lead to an expansion of the chain dimensions and a 6/5 power dependence of these dimensions on the number of segments in the chain. At moderate concentrations these interactions become screened from each other due to intermolecular interactions between segments on different chains. Diagrammatically we could represent two such interactions between three chains as:

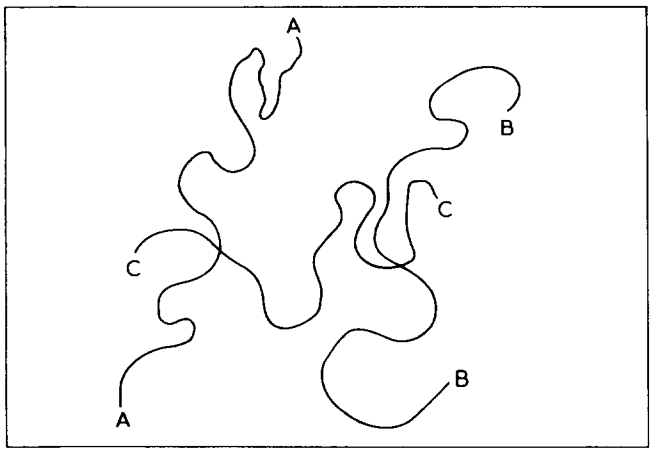

The distance along the chain was defined by Edwards[55] as the screening length, ξ. Effectively the portions of chain, C, on either side of the two interaction points have 'forgotten' the presence of that portion between the points, hence leading to an absence of excluded volume interaction. Within the length, ξ, excluded volume still plays a role but we shall see that as polymer concentration increases ξ decreases giving a qualitative explanation of the absence of excluded volume effects on bulk polymers.

Renormalization group theory of polymer solutions has provided a diagram in a temperature–concentration plane wherein specific regions of distinct polymer solution behaviour should be apparent[60]. *Figure 13* shows such a diagram and before proceeding further a brief description of the regions is given.

Region I' is a region where theta behaviour should prevail, i.e. unperturbed dimensions and no influence of temperature on chain dimensions. For a polymer of infinite molecular weight this region reduces to the origin. Thus: Region I, good solvent dilute regime, two parameter theories prevail here; Region II, semidilute solutions where chains overlap somewhat; Region III, concentrated solutions, with strong overlap of chains; Region IV, two phase region of the phase separation curve, the asymptotes of which are the lines $cM^{1/2} = 0$ and $-c^{**}$.

Equations for $\langle r^2\rangle_w$, the end-to-end distance of the polymer chain, and ξ, for each of regions I', I, II and III obtained by renormalization group theory scaling laws[60] and the analytical theories of Edwards[55,56] are given in *Table 6.*

Table 6 N.B. $\theta_T = T - \theta$

	Scaling laws		Analytical formulae	
Region	$\langle r^2\rangle$	ξ^2	$\langle r^2\rangle$	ξ^2
I'	N			
I	$N^{6/5}\theta_T^{2/5}$		$N^{6/5}\theta_T^{2/5}$	
II	$N\theta_T^{1/4}c^{-1/4}$	$c^{-3/2}\theta_T^{1/2}$	$C_\infty nl^2[1 +$	$\gamma c^{-1}\theta_T^{-1}$
III	N	c^{-2}	$Kc^{-1/2}\theta_T^{1/2}]$	

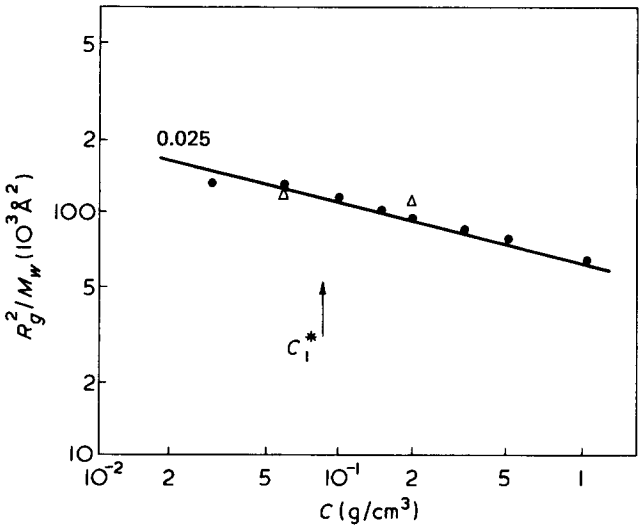

Figure 14 Log–log plot of R_g^2/M_W against c for PSD in PSH: ●, M_W = 1.14 x 10^5 and △, M_W = 5 x 10^5. [Reproduced from Daoud, M., Cotton, J. P., Farnoux, B., Jannink, G., Sarma, G., Benoit, H., Duplessix, R., Picot, C. and de Gennes, P. G. *Macromolecules* 1975, **8**, 804 by permission of the American Chemical Society ©]

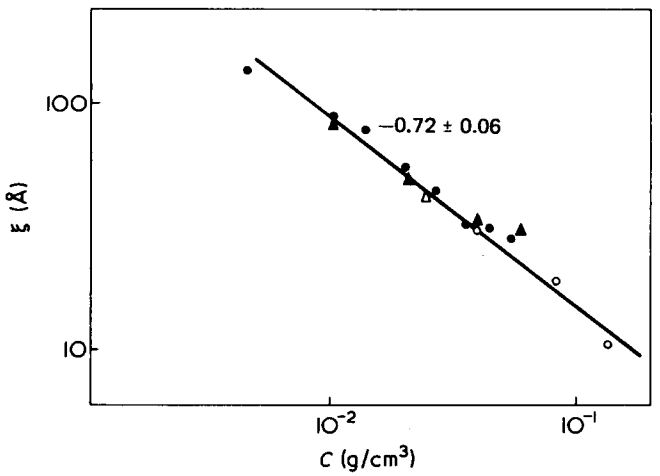

Figure 15 Log–log plot of ξ against c. PSH in deuterated benzene: ●, M_W = 2.1 x 10^6 and ▲, M_W = 6.5 x 10^5. PSD in carbon disulphide: ○, M_W = 5 x 10^5 and △, M_W = 1.1 x 10^6. [Reproduced from Daoud, M., Cotton, J. P., Farnoux, B., Jannink, G., Sarma, G., Benoit, H., Duplessix, R., Picot, C. and de Gennes, P. G. *Macromolecules* 1975, **8**, 804 by permission of the American Chemical Society ©]

The concentration dependence of chain dimensions in the semidilute region (II) has been studied by Cotton *et al.*[62] using polystyrene dissolved in carbon disulphide. Results for $\langle r^2\rangle_w$ and ξ are shown in *Figures 14* and *15* and the slopes from these log–log plots are in excellent agreement with the scaling law predictions of *Table 6*. Investigations[63] of the temperature dependence of chain dimensions have been made using polystyrene in cyclohexane solutions at temperatures between the θ point (30°C for PSD in C_6H_{12}) and ~70°C. Semidilute solutions (~15–20% PS wt/vol) again conform to scaling law behaviour as *Figure 16* for $\langle s^2\rangle_w$ shows. The initial θ region is clearly discernible and the slope of the temperature dependent portion of these results is ~0.26. For the same region of temperature and concentration ξ^2 was linear with $\theta_\tau^{-1/2}$ as expected from scaling laws.

Increasing the concentration to ~50% completely changes the behaviour and not in accordance with scaling laws (Region III–Region II of *Figure 13*). Results[64] for $\langle r^2\rangle_w$ (*Figure 17*) follow the behaviour described by Edwards' equation both above and down to 20° *below* the θ temperature. Furthermore, C_∞, the characteristic ratio, from the intercept in *Figure 17* is 9.7 ± 0.5 which compares well with values of 10.0 for polystyrene obtained by dilute solution viscometric studies. Additionally[65], ξ^{-2} in this region was linear in θ_τ as originally proposed by Edwards[55].

To some extent the breakdown of scaling laws in concentrated solutions is expected[57]. However, this must not detract from the undoubted power of scaling law techniques in their ability to predict *a priori* the different behaviour regions. Further theoretical developments will come with the publication of an extrapolation theory of polymer dimensions in solution at present being developed by Edwards and Jeffers[66].

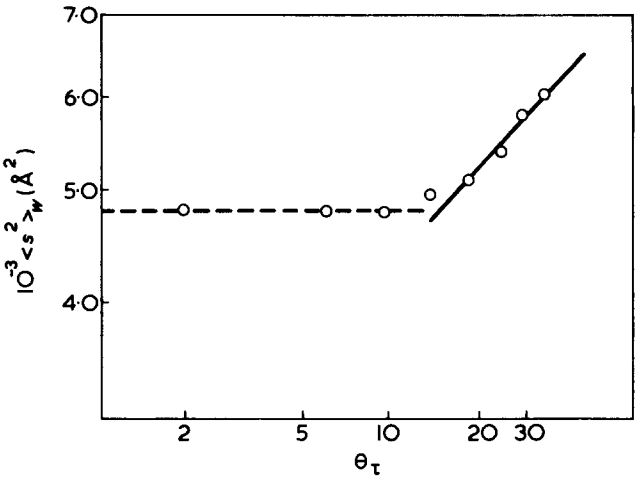

Figure 16 Plot of $\langle s^2\rangle$ against log θ_τ for a semidilute solution of polystyrene in cyclohexane. c = 19% w/v and M_W = 7.6 x 10^4. Slope −0.72 ± 0.06 [Reproduced from Richards, R. W., Maconnachie, A. and Allen, G. Polymer 1978, **19**, 266 ©]

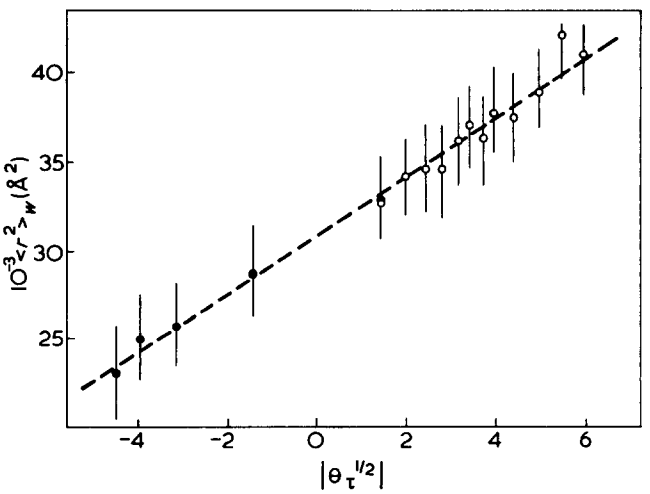

Figure 17 Plot of $\langle r^2\rangle$ against $|\theta_\tau^{1/2}|$ for polystyrene in cyclohexane. c = 47% w/v; M_W = 7.6 x 10^4. [Reproduced from Richards, R. W., Maconnachie, A. and Allen, G. *Polymer* 1978, **19**, 266 ©]

DYNAMICS OF POLYMER CHAINS

Introduction

During the past few years two new scattering techniques – neutron quasielastic scattering (NQES) and photon correlation spectroscopy (PCS) – have been used to obtain information about the dynamics of polymer chains. These new experimental techniques have been complemented by a new outlook on the theory of chain dynamics. Separately, neither NQES or PCS can cover the whole momentum transfer range necessary to check these theories. PCS is used mainly to measure the overall translational motion of polymer chains since $QR_g \ll 1$, where R_g is the root mean square radius of gyration $\langle s^2 \rangle^{1/2}$. On the other hand, NQES with $QR_g \geqslant 1$ observes motions which are related to segmental motion and the internal modes of the chain. Together these two techniques cover almost the whole of the relevant Q range.

In the first part of this section the theoretical predictions for NQES and PCS are briefly described. The theoretical treatments for NQES predict either the scattering law $S(\mathrm{Q}, \omega)$ or the behaviour of the full width at half maximum (*FWHM*) $\Delta\omega$ as a function of momentum transfer. To simplify the discussion the behaviour of $\Delta\omega$ as $f(Q)$ is used to compare experiment with theory. In the second and third parts the experimental results obtained using NQES are reviewed and comparisons made with theoretical predictions.

Theory

The scattering law $S(\mathbf{Q}, \omega)$ can be written as the Fourier transform of $I(\mathbf{Q}, t)$, the intermediate scattering law. $I(\mathbf{Q}, t)$ is essentially a time correlation function and is the Fourier transform of the pair correlation function $G(\mathbf{r}, t)$ or the self-correlation function $G_s(\mathbf{r}, t)$. Thus:

$$I(\mathbf{Q}, t) = \int \exp(i\mathbf{Q}.\mathbf{r})\, G(\mathbf{r}, t)\mathrm{d}\mathbf{r} \tag{45}$$

and

$$S(\mathbf{Q}, \omega) = \int \exp(i\omega t) I(\mathbf{Q}, t)\mathrm{d}t \tag{46}$$

In order to calculate $S(\mathbf{Q},\omega)$ it is necessary to first of all calculate $I(\mathbf{Q}, t)$ (in PCS $I(\mathbf{Q}, t)$ is measured directly). For a simple liquid the centre of mass motion can be described in terms of a self-diffusion coefficient, D, which is related to $I(\mathbf{Q}, t)$ by the expression (see Marshall and Lovesey[4]):

$$I(\mathbf{Q}, t) = \exp(-Q^2 Dt) \tag{47}$$

The scattering law calculated using equation (47) is therefore:

$$S(\mathbf{Q}, \omega) = \frac{\pi}{2} \frac{DQ^2}{\omega^2 + (DQ^2)^2} \tag{48}$$

At constant $\mathbf{Q}$, $S(\mathbf{Q}, \omega)$ will have a Lorentzian shape and a half-width $\Delta\omega \propto DQ^2$. Although equations (47) and (48) were calculated for simple liquids they are also applicable to the centre of mass motion or translational diffusion of large molecules (especially in dilute solution) if $QR_g \ll 1$.

To describe the motions of a polymer other than overall translational diffusion it is necessary to incorporate into any theory the special feature of the polymer chain, namely the connectivity of the monomer units. Using the bead-spring model of Rouse[67] and Zimm[68], de Gennes and Dubois-Violette[69,70] have calculated $I(\mathbf{Q}, t)$ for a dilute solution of a very long polymer in a θ solvent, i.e. under the constraint of random flight statistics. Another condition was imposed on $I(\mathbf{Q}, t)$ that it held only for long time behaviour. This is equivalent to small energy and momentum transfers in neutron scattering, i.e. $QR_g \gg 1 > Qd$, where d is the interatomic distance. The expressions calculated for $I(\mathbf{Q}, t)$ are:

$$I(\mathbf{Q}, t) = \exp\left[-Q^2 \frac{l^2}{3} \left(\frac{W}{\pi} |t|\right)^{1/2}\right] \tag{49}$$

for the Rouse limit (no hydrodynamic interactions) and:

$$I(\mathbf{Q}, t) = \exp\left[-Q^2 \frac{l^2}{6\pi} \Gamma\left(\frac{1}{3}\right) |\tilde{W}t|^{2/3}\right] \tag{50}$$

for Zimm type behaviour with hydrodynamic interactions. Equations (49) and (50) are for incoherent scattering. Similar expressions were calculated for coherent scattering. l is the step-length of the polymer, $W = 3k_BT/\pi\eta_0 dl^3$ and $\tilde{W} = 3k_BT/\pi\eta_0 l^3$, where η_0 is supposed to be the solvent viscosity. W^{-1} and $\tilde{W}^{-1}$ are correlation times of the order of 10^{10} to 10^{14} sec.

The peculiar time dependences $t^{1/2}$ and $t^{2/3}$ in the expressions for $I(\mathbf{Q}, t)$ give rise to a quite different dependence of $\Delta\omega$ on Q for $S(\mathbf{Q}, \omega)$. In the Rouse limit:

$$\Delta\omega_{\mathrm{inc}} \approx 0.01 Wl^4 Q^4 \tag{51}$$

for incoherent scattering, and:

$$\Delta\omega_{\mathrm{coh}} \approx 0.066 Wl^4 Q^4 \tag{52}$$

for coherent scattering, whereas in the Zimm limit:

$$\Delta\omega_{\mathrm{inc}} \approx 0.075 Wl^3 Q^3 \tag{53}$$

and

$$\Delta\omega_{\mathrm{coh}} \approx 0.055 Wl^3 Q^3 \tag{54}$$

Dubois-Violette and de Gennes[70] also considered the range of validity of the Rouse and Zimm limits. If

$$Ql \ll h^2$$

equations (53) and (54) apply and if

$$1 \gg Ql \gg h^2$$

where $h^2 = 6/\pi(d^2/l^2)$ equations (51) and (52) apply.

Another interesting point to note is that if the expression for $\tilde{W}$ is substituted into equation (50) then $I(\mathbf{Q}, t)$ will depend only on η_0, the solvent viscosity, and not the step-length. According to this statement the scattering law should be independent of chain chemistry, i.e. the same for all polymers. Akcasu and Gurol[71] using a bead-spring model and the projection operator technique have calculated $S_{\mathrm{coh}}(\mathbf{Q}, \omega)$ for dilute polymer solutions. The expressions arrived at are qualitatively the same as those of de Gennes[69,70] in the range of Q where equations (51) to (54) apply. For small $Q(QR_g \ll 1)$ they predict

$$\Delta\omega = 0.195 \frac{k_B T}{\eta_0 l (N)^{1/2}} Q^2 \quad (55)$$

where $Nl^2 = \langle r^2 \rangle$ the end-to-end distance of the chain and for large Q. ($Ql \gg 1$),

$$\Delta\omega = \frac{k_B T}{F} Q^2 \quad (56)$$

At large Q values the width is mainly governed by the friction coefficient of the segment, F, and at small Q by the solvent viscosity η_0. At intermediate values of Q Akcasu and Gurol[71] obtained:

$$\Delta\omega = \frac{l^2 k_B T}{12F} Q^4 \quad (57)$$

in the Rouse limit, and:

$$\Delta\omega = 0.55 \frac{k_B T}{\eta} Q^3 \quad (58)$$

when hydrodynamic effects are included. Equations (57) and (58) agree with de Gennes' and Dubois-Violettes'[69,70] calculations. Using a different model, that of a freely jointed chain, Akcasu and Higgins[72] recalculated the behaviour of $\Delta\omega$ as a function of Q. The expression obtained was:

$$\Delta\omega = \frac{k_B T}{f} Q^2 F(Z, X, N) \quad (59)$$

where $Z = f/\eta_0 p$, f is the friction coefficient per segment, p is the bond length of a freely jointed chain of N bonds in length and $X = Qp$. In the limits of high and low Q the form of $F(Z, X, N)$ is such that equation (59) reduces to equations (55) and (58), respectively. Equation (59) also describes the transition region between Q^3 and Q^2 behaviour at intermediate values of Q. Jannink and Saint-James[73] have also calculated $\Delta\omega$. Using the Rouse model, but unlike de Gennes who used the diffusion equation approach of Zimm, they have used the coupled Langevin equations used by Bueche[74]. The result essentially agrees with that obtained by de Gennes giving a Q^4 dependence for $\Delta\omega$.

The theoretical calculations described so far all assume that the polymer chain is completely flexible. Jannink and Summerfield[75] introduced the notion of hindered motion in the chain into their calculations of the incoherent scattering law. In the long t limit for a completely flexible chain they obtained the expression of de Gennes, i.e. $I(\mathbf{Q}, t) \propto \exp(-At^{1/2})$. Assuming the chain is not completely flexible an expression was obtained which included $\bar{u}$, the average of the cosine of the angle between adjacent segments. The introduction of finite values of $\bar{u}$ has the effect of smoothing out the transition from t behaviour at small time to $t^{1/2}$ at long time and also shifts the crossover region to longer values of t. This is equivalent to saying that the changeover from Q^4 to Q^2 behaviour will occur at lower values of Q if the chain is stiff.

Jannink and Summerfield[75] also calculated the half width dependence when $l \to 0$ and $\bar{u} \to 1$, the Kratky–Porod limit, and in this case:

$$\Delta\omega \propto (Qa)^{8/3} \quad (60)$$

where a is the persistence length.

All the above mentioned calculations refer to single chain behaviour. Jannink and de Gennes[76] have calculated the coherent scattering law for a semidilute solution of polymer chains where the radius of gyration of each coil is considered to be much larger than the distance between neighbouring coils. An expression for $\Delta\omega$ was calculated of the form:

$$\Delta\omega = \Delta\omega_R [1 + (\xi^2/Q^2)] \quad (61)$$

where $\Delta\omega_R$ is the half width computed by de Gennes[69] which is proportional to Q^4 and ξ^{-1} is the static screening length. If $Q \ll \xi^{-1}$ then equation (61) becomes $\Delta\omega \propto Q^2$, therefore at low Q, $\Delta\omega \propto Q^2$ and at $Q > \xi^{-1}$, $\Delta\omega \propto Q^4$.

Recently, de Gennes[77] has used scaling arguments to look at the dynamics of long, flexible chains in good solvents where entanglements are present. Two regimes are identified: (i) when $Q < \xi^{-1}$ a cooperative diffusion coefficient D_c can be measured and (ii) when $Q > \xi^{-1}$ single chain behaviour should be observed with $\Delta\omega \propto Q^3$.

For polymer chains in a θ solvent Brochard and de Gennes[78] considered the dynamics of a single chain, which was strongly self-entangled, and semidilute chains. In the Q range $QR_g \gg 1$ then $\Delta\omega \propto Q^3$ but if $R_g^{-1} \ll Q \ll g^{-1}$, where g is the distance between entanglements, then $\Delta\omega \propto Q$, a most unusual functional dependence.

Some attention has been paid to the effects of stretching a polymer chain on its dynamics by de Gennes[69] and Pincus[79]. De Gennes[69] calculated the effect of stretching on $S_{coh}(\mathbf{Q}, \omega)$ and concluded that the width $\Delta\omega$ would increase and that it would be proportional to Q^2 instead of Q^4 in the Rouse limit. Pincus[79] using scaling arguments derived the Q dependence of $\Delta\omega$ for incoherent scattering and in the regime $\xi_t^{-1} \gg Q \gg R_g^{-1}$ predicted that $\Delta\omega \propto Q^{10/3}$. ξ_t is the tensile screening length.

Experimental results

Although the theories described above refer to dilute polymer solutions, historically the first NQES measurements were made on bulk polymers. NQES has been used for many years to study simple molecule dynamics but it is only during the last five years that measurements have been published of NQES from bulk polymers and polymer solutions.

Bulk polymers. The first measurements of NQES from bulk amorphous polymers were made by Allen and coworkers[80]. Measurements were made of the incoherent NQES using a medium resolution *TOF* machine. A number of linear dimethyl siloxanes were studied, oligomers and polymers, with the degree of polymerization, n, varying from 3 to 2000. Five cyclic dimethyl siloxanes were also studied, the number of silicons in the rings varying from 3 to 18. The scattering was analysed in terms of the model for a simple liquid (Equation 48) and values of the 'effective' diffusion coefficient, D_{eff}, were calculated from the data. The values of D_{eff} were of the order of 10^{-5} cm^2/sec, similar to small molecule diffusion coefficients.

It was found that as n increased the value of D_{eff} decreased until it reached an asymptotic value at about $n = 20$. Similar values of D_{eff} were measured for the larger cyclic siloxanes. It was also found that a small amount of cross-linking did not affect the value of D_{eff}. A value of $n = 70$ for the asymptotic behaviour has been found for poly (ethylene oxide) and attributed to the increased stiffness of the chain[81].

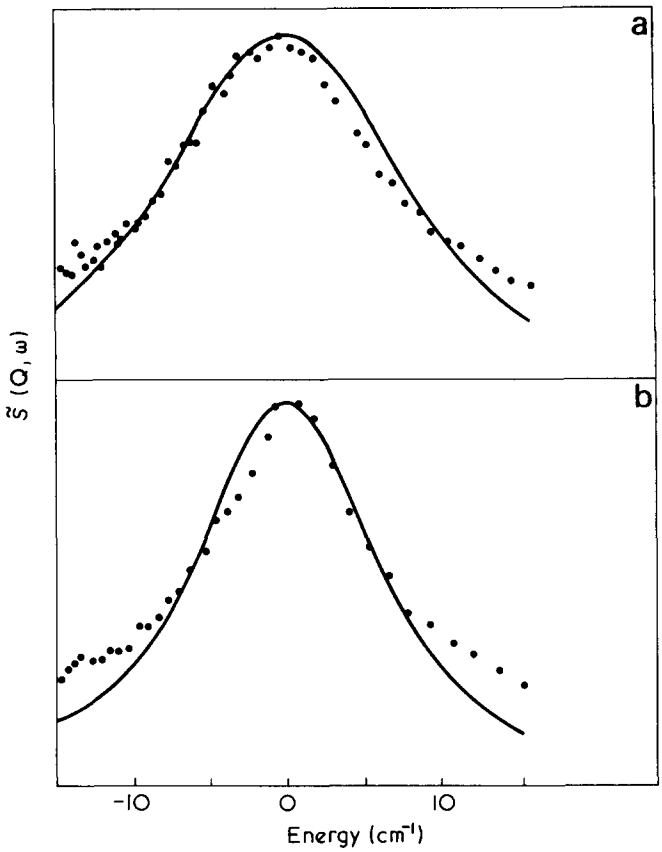

Figure 18 Neutron scattering profile for (a) a 4 unit; and (b) a 2000 unit linear poly(dimethyl siloxane) chain at 90° of scatter. ———, Best fit Voigt function; ●, experimental data. [Reproduced from Allen, G., Brier, P. N., Goodyear, G. and Higgins, J. S *Faraday Symp. Chem. Soc.* 1972, 6, 169 by permission of the Chemical Society ©]

Table 7 Effective diffusion coefficients and activation energies

Polymer	$D_{eff} \times 10^5$ at 20°C (cm^2/sec)	E_A (kJ/mol)
Poly(dimethyl siloxane)	2.09	7.5
Poly(methyl phenyl siloxane)	0.62	11.4
Polyisobutylene	0.04*	22.0
Poly(propylene oxide)	0.27*	19.0
Poly(ethylene oxide)	0.20*	22.0

*Extrapolated values

Assuming a simple Arrhenius dependence for D_{eff} of the form $D_{eff} = A \exp(-E_A/RT)$, activation energies were calculated of the order of 2 kcal/mol for both the short and long chain siloxanes. The authors concluded that the motion measured by NQES was probably segmental motion of the polymer chains. The Lorentzian signal shape, in equation (48), was found to underestimate the intensity of the signal from the polymer in the wings of the NQES. This is illustrated in *Figure 18*. At high Q there was evidence of a non-linear dependence of $\Delta\omega$ on Q^2.

In a subsequent paper, Allen and coworkers[82] studied a number of different polymers, with and without side groups above their glass transition temperatures. Using the simple diffusion model measurements were made of D_{eff} and the activation energy calculated E_A for poly(methyl phenyl siloxane), poly(propylene oxide), poly(ethylene oxide) and polyisobutylene. Values of D_{eff} and E_A are shown in *Table 7*. In order to establish whether or not side group motion contributed to the measured scattering poly(propylene oxide) was studied with: (a) the CH_3 group deuterated and (b) the backbone deuterated as well as (c) the normal hydrogenous polymer. All three sets of data could be placed on the same curve indicating that it was the backbone motion which predominated. The activation energies were compared with data from relaxation and viscosity measurements. It was found that $E_{viscosity} > E_{relaxation} > E_{neutron}$.

Further measurements have been made on poly(dimethyl siloxane) (PDMS)[83,84] using high resolution spectrometers at low Q down to $Q \sim 0.1$ Å^{-1}. Larsson[85] had suggested that the NQES from a polymer should have two components due to translational and rotational motion as is the case with liquid crystals. No evidence was found of this type of behaviour.

Attempts have been made[84] to fit a model of the dynamics of a polymer chain to the data for PDMS. Data collected from machines with different resolutions and covering a range of Q of 0.15 to 2 Å^{-1} and 3 decades of $\Delta\omega$ have been fitted using de Gennes' model for a single chain in the Rouse limit (see equation 49). In *Figure 19* the broadening $\Delta\omega$, calculated using a Q^4 dependent model is shown as a function of Q, the slope is equal to 4. Although the fit was very much improved compared with that for simple diffusion it was noted that the model still tended to underestimate the intensity in the wings of the NQES peak. The de Gennes model is valid for long time behaviour and no short time contribution is included which could account for the extra intensity.

High resolution measurements carried out on poly (ethylene oxide)[81] (PEO) were also fitted to the de Gennes

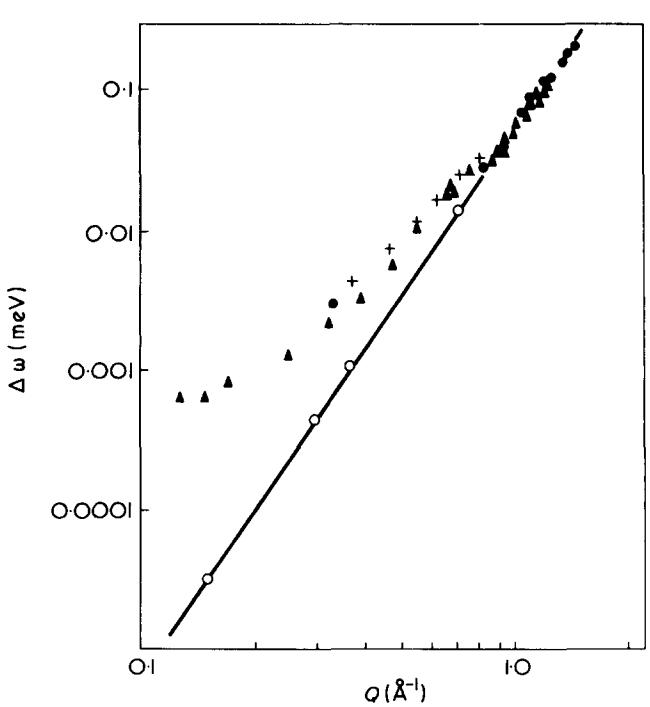

Figure 19 Log–log plot of $\Delta\omega$ against Q. $\Delta\omega$ is the half width of the best fit curves for the Q model. ● and +, IN5, 8 Å incident beam; ▲, IN5, 10 Å incident beam; ⊙ IN10, 6.2 Å incident beam. A line with slope = 4 is indicated. [Reproduced from Higgins, J. S., Ghosh, R. E. and Howells, W. S. *J. Chem. Soc. (Faraday Trans. 2)* 1977, 73, 40 by permission of the Chemical Society ©]

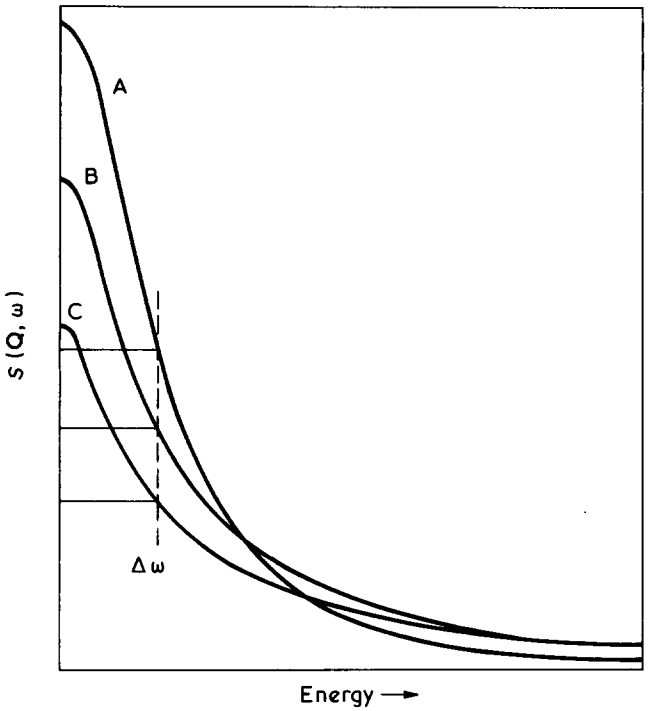

Figure 20 The shape of $S(Q, \omega)$ for the three model correlation functions: A, Lorentzian $\Delta\omega \propto Q^2$; B, Zimm, $\Delta\omega \propto Q^3$; Rouse, $\Delta\omega \propto Q^4$. [Reproduced from Higgins, J. S., Ghosh, R. E., Allen, G., Farnoux, B. and Weill, G. *Chem. Phys. Lett.* submitted for publication, by permission of the North Holland Publishing Co. ©]

Q^4 model, but in this case the limiting slope was only 3.3. As in the case of polymer solutions one would expect the variation $\Delta\omega$ with Q to change as Q increases or decreases. It is probable that in the range of Q used, because of the differences in segment length of PDMS and PEO, the PEO chain has not yet reached the limiting flexibility which generates Q^4 behaviour.

Measurements have also been made on carbon black filled natural rubber and polybutadiene[86]. D_{eff} values showed little or no variation as the filler loading increased which was interpreted as meaning that no appreciable layer of immobilized material was present.

Using stretched crosslinked *cis*-polybutadiene[86] measurements have been made of D_{eff} parallel and perpendicular to the stretch direction as a function of extension ratio but no significant differences caused by stretching were found.

Polymer solutions. In order to test the validity of the models proposed by de Gennes and Dubois-Violette[69,70] it is necessary to measure the NQES from dilute polymer solutions. Using polytetrahydrofuran (PTHF) and its deuterated analogue (PTDF) in CS_2, Allen *et al.*[87] were able to measure both the incoherent and coherent NQES from a dilute polymer solution. The scattering from PTHF in CS_2 is almost entirely incoherent and that from PTDF in CS_2 almost entirely coherent. The NQES from each solution was measured on two machines of very different resolution, IN10 and IN5 at the ILL. IN10, the backscattering spectrometer, has a very limited energy window but very high resolution and so it is particularly sensitive to the shape of the central part of $S(\mathbf{Q}, \omega)$. On the other hand, IN5, a *TOF* spectrometer, has an unlimited energy range but coarser resolution so it is more sensitive to the shape of the wings of $S(\mathbf{Q}, \omega)$. If the half widths measured in the same Q range on the two machines agree then it points to the fact that the right model has been chosen. A good illustration of this point can be found in ref 84 where the scattering from water and PDMS was fitted to a Lorentzian and $\Delta\omega$ plotted as a function of Q. Only in the case of water can a line be drawn through the data from both machines.

The solution data were fitted to three models of the scattering law, of the following type: (1) a Lorentzian ($\Delta\omega \propto Q^2$); (2) a Zimm type ($\Delta\omega \propto Q^3$); (3) a Rouse type ($\Delta\omega \propto Q^4$). In *Figure 20* the shapes of these three laws are drawn for the same $\Delta\omega$. In order to estimate which model best fitted the data a number of parameters were calculated which should be sensitive to the form of $S(\mathbf{Q}, \omega)$: (1) The half width of the scattering law should be proportional to Q^β; (2) the peak height $S(\mathbf{Q}, 0) \propto Q^\alpha$, and (3) the area under the peak

$$\int S(\mathbf{Q}, \omega) d\omega \propto Q^{\alpha+\beta}$$

where for incoherent scattering $\alpha = -\beta$ and for coherent scattering $\alpha = -(\beta + 2)$. Using these criteria it was found that although there was general disagreement with the Rouse model it was not clear-cut which of the other two models best fitted the data. A range of β values was measured between 1.95 and 3.12. The data tended to favour the Q^3-dependent Zimm model. Various reasons were given to try to explain the discrepancies between the theoretical and experimental scattering laws. The experiments were not performed at the θ temperature and the molecular weight of the polymers was low $\sim 15 \times 10^3$ although strictly the theories of de Gennes hold for infinitely long chains in a θ solvent. Another point was that the same law had been fitted over the entire Q range including values of $Ql > 1$. In the range $Ql > 1$ it is quite possible that a Q^2 law will hold whereas Q^3 will hold at lower Q values.

In order to clarify a number of these points further measurements were made by Higgins *et al.*[88] on high and low molecular weight PTHF and PTDF in CS_2 near the θ point. No molecular weight dependence of the NQES was found. The NQES from polystyrene (PSH) and deuterated polystyrene (PSD) in CS_2 was also measured at the θ point. According to Dubois-Violette and de Gennes[70], $\Delta\omega$ should be independent of the chemical structure but this was not found to be true for the two polymers. The difference in chemical structure of the two polymers could manifest itself in two ways: (a) the step lengths, l, of the two polymers are different or (b) η_0 is really a microscopic viscosity involving interactions between polymer and solvents.

The conclusions which were reached were that the incoherent scattering favoured the Zimm model whereas the coherent scattering tended towards the Lorentzian form of the law. The problem still remains that $Ql = 1$ and this will only be changed when new techniques are available to achieve lower Q values in the range $R_g^{-1} < Q < l^{-1}$.

The coherent NQES data from PTDF and PSD discussed above[87,88] has also been used by Akcasu and Higgins[72] in order to test the validity of their theoretical calculation using a freely jointed chain model. By using the fact that the data seem to be in the transition region from Q^3 to Q^2 behaviour, an effective bond length, p, and the associated friction coefficient per segment, f, were estimated. The data for PTDF and PSD was fitted to the theory and the best fit was achieved using for PTDF, p = 3.8 Å, and for PSD, p = 6.3 Å.

All the measurements discussed so far have been made on dilute polymer solutions. Maconnachie *et al.*[81] have

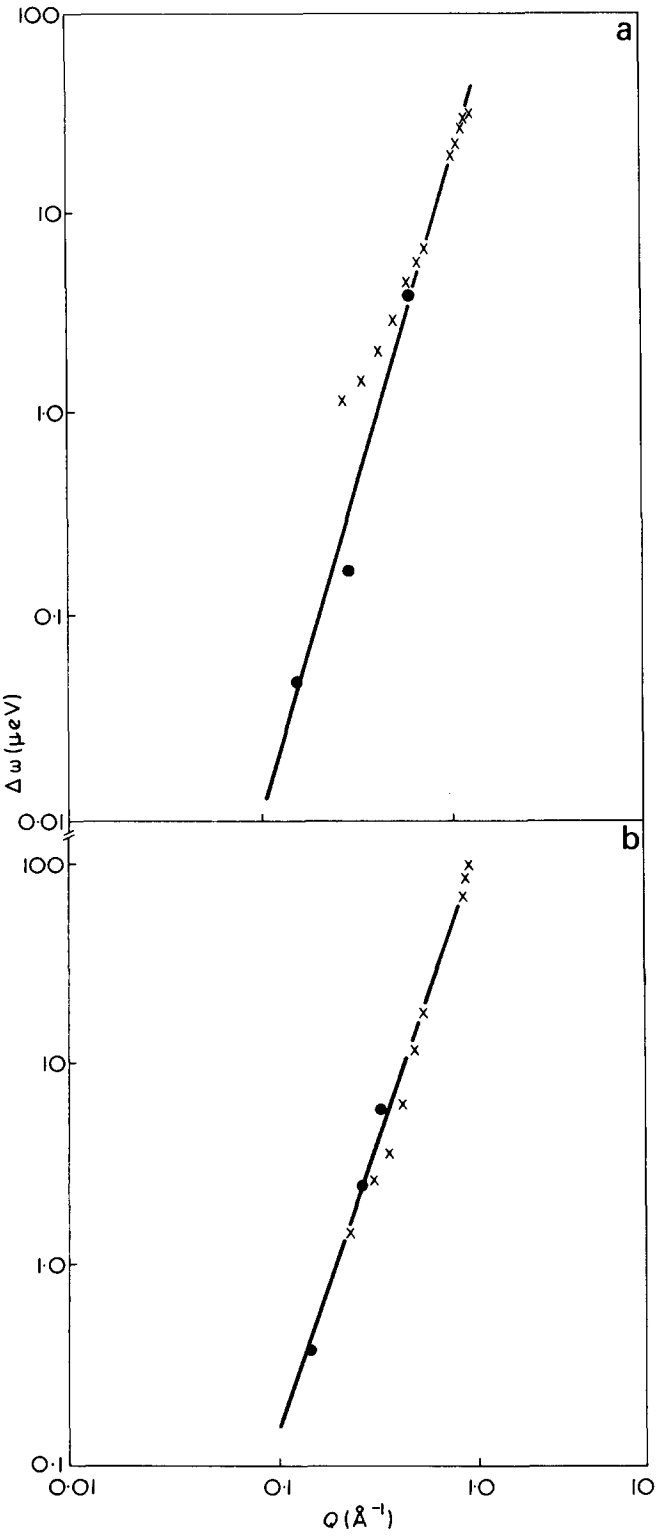

Figure 21 Log–log plots of $\Delta\omega$ as a function of Q for (a) bulk PEO, best fit model Q^4 slope = 3.3, and (b) PEO in D_2O, concentration 3 mol D_2O/monomer, best fit model Q^3, slope = 2.9. [Reproduced from Maconnachie, A., Vasudevan, P. and Allen, G. *Polymer* 1978, **19**, 33 ©]

measured the effect of a small amount of water on the dynamics of poly(ethylene oxide) (PEO). The most dilute solution studied contained 30% polymer. Using the fitting techniques described previously[84,87,89] the best fit to the incoherent NQES was found to vary from Rouse (for the bulk polymer) to the Zimm model as the amount of water was increased. This point is illustrated in *Figure 21*. Low resolution measurements were analysed using a simple Lorentzian. A plot of D_{eff} of PEO in PEO/D_2O against concentration was found to change shape when approximately 1 mol of D_2O/monomer was present. Similar behaviour was observed for the water in the solution.

PEO behaved quite normally in toluene, D_{eff} increasing rapidly as soon as the solvent was added. The behaviour of PEO in water and toluene as measured by neutron scattering was mirrored in viscosity measurements made on the same solutions. The conclusion was drawn that PEO and water form a 1:1 hydration complex.

INELASTIC NEUTRON SCATTERING STUDIES OF SIDE GROUP MOTION IN POLYMERS

Introduction

At temperatures below the glass transition, polymers no longer exhibit the long range motion characteristic of rubbers. However, this does not mean that *all* molecular motion has ceased. It is the remaining motions which are responsible for the various loss phenomena in polymers which may be observed as minima in n.m.r. spin lattice relaxation or maxima in mechanical and dielectric loss measurements. For convenience the relaxations are classified according to the temperature or frequency region in which they are observed[89]. The glass transition is generally termed the α transition being the relaxation which occurs at the highest temperature (or the lowest frequency). β, γ and δ relaxations take place at decreasing temperature (or increasing frequency at a fixed temperature). Main chain Brownian motion is thought to be responsible for the β relaxation which, for typical polymers, is generally between 200 and 300K. Between 80 and 200K are found the γ relaxations, which are attributed to long side chains with coupled rotors such as propyl groups. We will not deal with these relaxations here, but will be particularly concerned with low temperature (<80K) δ relaxations, which are due to the torsions of methyl, ethyl or phenyl groups pendant to the main chain. Detailed reviews of these and other relaxation processes are available elsewhere[89–92].

Although the torsional modes of groups involved in δ relaxations are i.r. and Raman active, they are very weak. We hope to show that neutron inelastic incoherent spectroscopy (NIIS) is a technique extremely well suited to study such modes.

Theory

This section is restricted to torsional oscillations only. Detailed derivations of the equations will not be presented but are available in the publications of Marshall and Lovesey[4], Boutin and Yip[93] and Allen and Higgins[6]. Equation (25) can be re-written as:

$$\left(\frac{d^2\sigma}{d\Omega dE}\right)_{\text{inc}} = N\frac{k}{k_0}\frac{\sigma_{\text{inc}}}{4\pi}S_{\text{inc}}(\mathbf{Q},\omega)$$

since

$$\sigma_{\text{inc}} = 4\pi(\overline{b^2} - \overline{b}^2)$$

For one atom of mass m, whose frequency of a particular normal mode of motion is ω_j, then,

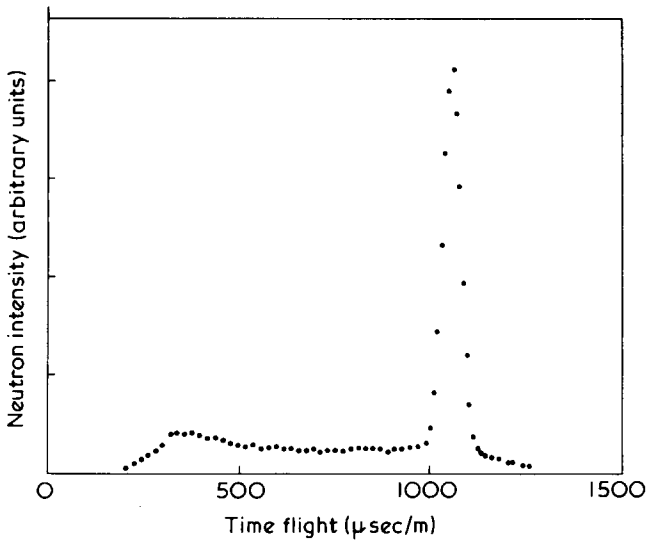

Figure 22 Time of flight spectrum obtained from PMMA at 90° of scatter

$$S_{inc}(\mathbf{Q}, \omega) = \left(\frac{QU_j}{2\omega_j m}\right)^2 \frac{\exp(-\hbar\omega_j/k_B T)}{1 - \exp(-\hbar\omega_j/kT)} \times \exp(-2W)\delta(E \pm \hbar\omega_j) \quad (61)$$

where k_B is the Boltzmann constant, E the energy, Q the momentum transfer on scattering (see equation 2), U_j is the displacement vector of the moving atom and $\exp(-2W)$ is the Debye–Waller factor which contains both Q and U_j.

Clearly from equation (45) provided the particular mode, j, is not subject to dispersion by coupling with other normal modes, then the vibrational transitions are represented by the delta function $\{\delta(E \pm \hbar\omega_j)\}$. The intensity of the vibrational band is dependent on several factors: (i) the momentum transfer, Q, and since Q is dependent on angle the spectrum varies with angle of scattering; (ii) the displacement vector, U_j, and hence the amplitude of normal vibrational mode; (iii) the value of the incoherent scattering cross-section σ_{inc} of the atom being observed (see equation 18 above). Combination of (ii) and (iii) results in the NIIS from common polymers being dominated by hydrogen atom scattering, especially from those normal modes in which the hydrogen atoms have large amplitudes of motion. Since the vibrational bands are Q dependent, they may not be coincident with those derived from Raman spectra at $Q = 0$. Direct comparison with Raman spectra is obtained by using the hydrogen amplitude weighted density of vibrational states[94,95]. This subject is discussed by Kittel[96].

For solids the distribution function, $\rho(\omega)$, is:

$$\rho(\omega) = \frac{\hbar\omega_j}{k_B T} \sinh \frac{h\omega}{2k_B T} \lim_{Q \to 0} \frac{S_{inc}(\mathbf{Q}, \omega)}{Q^2} \quad (62)$$

Data for $S_{inc}(\mathbf{Q}, \omega)$ must then be gathered over a number of angles and extrapolated to zero Q. Generally, computational routines are available which carry out this extrapolation on the primary data which also normalizes all the data to a vanadium calibration. The application of deuterated polymers in coherent scattering has been discussed above in conjunction with SANS. Deuteration of polymers also plays an important role in NIIS. By selectively deuterating the polymer molecule it is possible to assign the various peaks in the spectra to the group motions which characterize particular normal modes. Since the incoherent scattering cross-section of deuterium is much less than that of hydrogen, comparison of spectra of hydrogenated and deuterated samples of the same polymer enables identification of group motions.

Experimental results

NIIS studies of polymers have advantages and disadvantages. A clear advantage is that the spectrum is dominated by scattering from protons. Secondly, since scattering is due to a neutron–nucleus interaction, the selection rules differ from those prevailing in optical spectroscopy (see above). There are, however disadvantages from the experimental point of view which include: (1) poorer resolution available in NIIS; (2) high cost of obtaining such spectra.

All of the NIIS data so far reported for polymers have been concerned with methyl or phenyl groups, i.e. symmetric top molecules. To our knowledge no data on asymmetric rotors has been published, the extraction of rotational barrier heights from data on such rotors is a formidable problem[97,98].

Methyl groups on polymer chains. Extensive NIIS investigations have been made on poly(methyl methacrylate) (PMMA)[99,100]. *Figure 22* shows a time of flight spectrum for PMMA at a scattering angle of 90° the frequency distribution function obtained is shown in *Figure 23*. Assignment of the various peaks to particular methyl groups can be made by comparing the spectra in *Figure 23* for the following polymethacrylates:

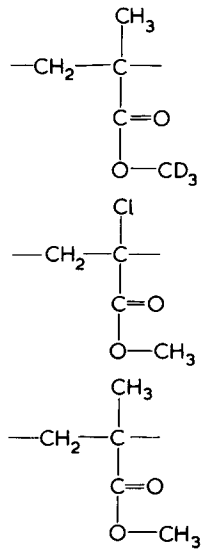

Ester deuterated PMMA

Poly (α-chloromethacrylate)

PMMA

Swelling the samples slightly with $CDCl_3$ produced no shift in the band positions, good evidence for the absence of strong dispersion.

From these spectra the following assignments were made; the broad band centred at 100 cm^{-1} was assigned to the ester methyl torsion by comparing spectra A and C. Comparison of spectra B and C, allowed assignment of the band at ~250 cm^{-1} to the α methyl group, this value being subsequently refined to 300 cm^{-1}.

The barrier to internal rotation of the methyl group (V_3) was calculated by using the Mathieu form of the Schrödinger wave equation in the following way. For hindered internal rotation about a single bond, the potential energy opposing rotation is a function of ϕ, the angle of

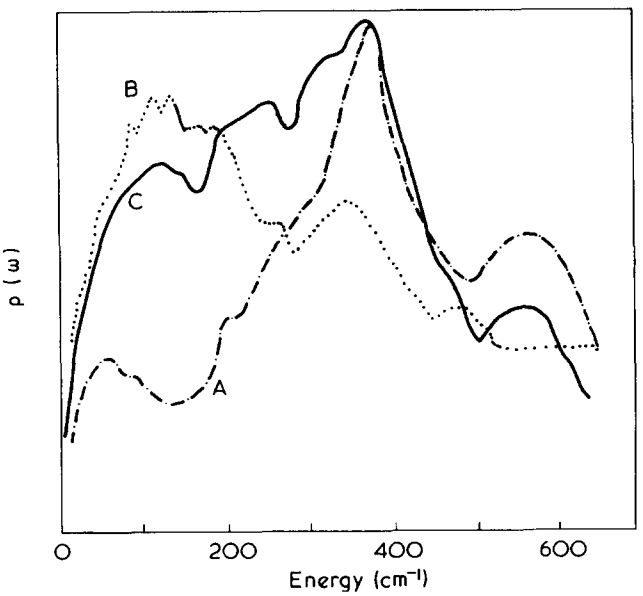

Figure 23 Frequency distribution $\rho(\omega)$ as a function of energy for: A, — · — · —, poly(methylmethacrylate — $COOCD_3$) (I); B, ●, poly(α-chloromethacrylate) (II) and C, ———, poly(methylmethacrylate) (III). [Reproduced from Higgins, J. S., Allen, G. and Brier, P. N. *Polymer* 1972, **13**, 157 ©]

rotation. We may write for a methyl group which has three fold symmetry:

$$V(\phi) = (V_3/2)(1 - \cos 3\phi) \tag{63}$$

The Schrödinger wave equation in one dimension can now be written as:

$$F\frac{\partial^2 Q_{\nu\sigma}(\phi)}{\partial\phi^2} + \left[E_{\nu\sigma} - \frac{V_3}{2}(1 - \cos 3\phi)\right] Q_{\nu\sigma}\phi = 0 \tag{64}$$

F contains the reduced moment of inertia of the side group; $E_{\nu\sigma}$ are the torsional energy levels of vibrational quantum number ν and index σ (see below). The Mathieu equation may be written as:

$$\frac{\partial^2 y}{\partial x^2} + (b - S\cos^2 x)y = 0 \tag{65}$$

Equations (64) and (65) can be transformed to each other by noting that;

$$Q_{\nu\sigma}(\phi) = y$$

$$3\phi + \pi = 2x$$

$$V_3 = (3^2/4)FS \tag{66}$$

$$E_{\nu\sigma} = (3^2/4)Fb$$

Considering only a transition of $\nu = 0 \rightarrow \nu = 1$ and for the moment disregarding σ (in most cases this is justifiable for transitions between lower energy levels) then

$$E_1 - E_0 = \frac{3^2}{4}F(b_1 - b_0)$$

$$= \hbar c\omega_{0-1}$$

where $\hbar = h/2\pi$, c = velocity of light *in vacuo* and ω_{0-1} is the wave number (in cm^{-1}) of the vibration. Therefore:

$$b_1 - b_0 = 4\hbar c\omega_{0-1}/3^2F \tag{67}$$

Values of b are tabulated as a function of S[101], and hence the value of S corresponding to $b_1 - b_0$ can be interpolated. V_3 can then be calculated from equation (66).

NIIS torsional frequencies and the barrier heights calculated from them for a number of methyl group containing polymers are given in *Table 8*, also included are activation energies from relaxation measurements where available. Comparison of activation energies and V_3 values supports the contention that methyl group rotation is responsible for the low temperature relaxation processes [cf poly(propylene oxide), and poly(dimethyl siloxane)]. Discrepancies are most apparent for PMMA, but these can be improved when account is taken of quantum mechanical tunnelling[103,104].

Where a particle passes through a region of potential energy greater than its own kinetic energy, the phenomenon of quantum mechanical tunnelling occurs. It arises where the wave functions each side of a potential barrier have significant amplitude across the barrier. For symmetric rotors such as methyl groups, conditions for such tunnelling are especially favourable since the energy levels are identical in each potential well. Methyl group tunnelling in PMMA contributes to viscoelastic relaxations[105,106] and its participation in other processes is summarized by Sauer[89]. Tunnelling results in activation energies obtained from a classical Arrhenius equation of the bulk relaxation process being too low. Corrections to such activation energies by the method of Stejskal and Gutowsky[107] produces much closer agreement with V_3 values for PMMA from NIIS (*Table 9*). The index σ in the torsional wave equation, equation (64), characterizes the symmetry of the wave function $Q_{\nu\sigma}(\phi)$. Full solution of equation (64) shows that the energy level ν is split into non-degenerate A and doubly degenerate E sub-levels, each of which have slightly different energies. For high barriers to rotation this splitting is negligible, as the barrier

Table 8

	ν_{tor} (cm^{-1})	V_3 kJ mol^{-1}	E_A kJ mol^{-1}
Methyl methacrylate[97]			
—OCH_3 (all isomers)	100	4.2	Very low
α—CH_3 isotactic	300	23	16
syndiotactic	360	33	23–35
Propylene oxide[97]	230	13	15.9
—methylstyrene[98]			
—heterotactic	380	37	
head-to-head	300	13	
Vinyl ether[98]	100	2.5	
Dimethyl siloxane[98]	165	6.9	8–10[89]
—$P(CH_3)_2$ = N—[98]	240	15	
4—methyl pentene[98]	240	15	1.7[100]
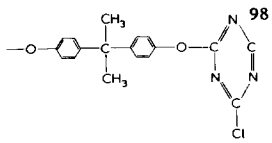 [98]	~300	~23	
Isobutene[98]	305	24	

Table 9 Corrections to barrier heights from quantum mechanical tunnelling and barrier heights from NIIS for PMMA samples

Group	E_A (kJ/mol)	E_A(Tunnel) (kJ/mol)	V_3 neutrons (kJ/mol)
α–CH_3 syndiotactic	23–25	29	33
α–CH_3 isotactic	16	22.6	23
OCH_3	Low	8.4	4.2

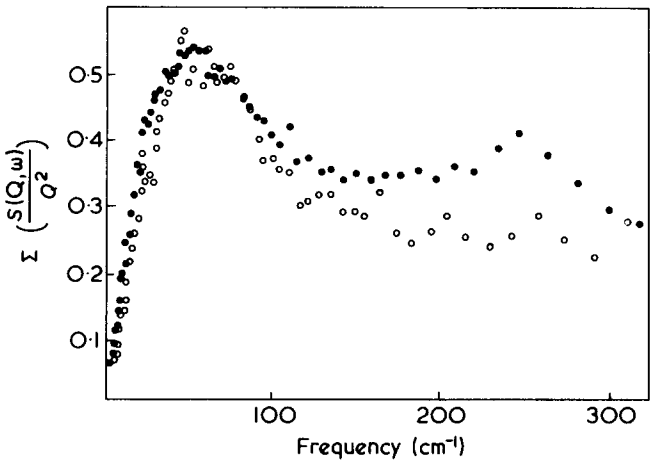

Figure 24 $\Sigma(S(Q,\omega)/Q^2)$ as a function of energy for ●, $-CH(C_6H_5)CH_2-$ and ○, $-CD(C_6H_5)CD_2$. [Reproduced from Spells, S. J. Shepherd, I. W. and Wright, C. J. *Polymer* 1977, 18, 905 ©]

height decreases it becomes more important. For the ester methyl group of PMMA calculations show that for a three-fold barrier this splitting should be about 2 μeV (≡2 x 10^{-4} kJ/mol) for the lowest energy level. This range of energy transfer can in principle be measured on the back-scattering instrument discussed above. Attempts to do so using amorphous and crystalline isotactic PMMA have been unsuccessful. This may be due to either imperfect crystallinity or the barrier being of higher order than 3-fold (a six-fold barrier would result in a splitting of ~200 μeV).

From *Table 8* the influence of stereochemistry on methyl group torsion can be discerned. Allen *et al.*[100] attribute the lower torsional frequency in head-to-head poly(α-methylstyrene) to steric hindrance forcing the main chain substituents into a *trans* conformation.

Phenyl groups. Much work has been reported on the n.m.r. mechanical and dielectric relaxations of polystyrene and has been surveyed in recent publications[108,109]. Alongside this experimental work, theoretical calculations of the barrier to internal rotation of the phenyl group in polystyrene has also been reported[110]. A variety of relaxations below the glass transition temperature have been reported and variously interpreted. Consequently the position is by no means as clear cut as in the case of PMMA. Because of this, a summary only of the scanty NIIS data (and associated data from Raman work) is presented here.

The only published work on NIIS from polystyrene and its homologues is that due to Spells, Shepherd and Wright[111] and Wright and Allen[112].

Raman work by Kim and coworkers[115] agrees with the more recent work of Spells *et al.* Both groups find a broad intense Raman band at ~60 cm^{-1}. By examining polystyrenes with substituted phenyl groups and noting the decrease in intensity of this band with increasing side group mass, Spells, Shepherd and Wright[111] attribute this band to phenyl group torsion. The same band is also plainly evident in the NIIS spectra of isotactic polystyrene shown in *Figure 24*. Also evident here are bands at ~30 and 250 cm^{-1}. Deuterating the main chain produces spectrum B, which shows a marked reduction in intensity of the 250 cm^{-1} band which therefore seems to be due to main chain vibrations. Attempts[114] have been made to determine the influence of steric crowding on 60 cm^{-1} band by using alternating copolymers of styrene–1,-1-diphenylethylene (IV) and styrene–*trans*-stilbene: (V)

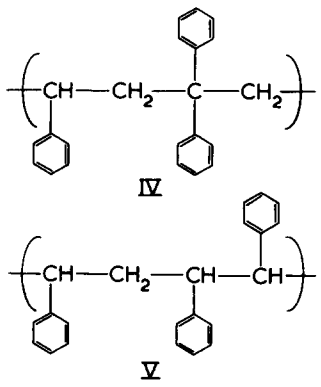

No measurable shift was observed.

Finally, in common with PMMA, polystyrene has a much higher specific heat at low temperature than that predicted by the Debye model. This has been attributed to phenyl groups in voids present in the structure acting as Einstein oscillators[115]. A high resolution NIIS investigation of polystyrene to detect such oscillators was however unfruitful[116].

FUTURE DEVELOPMENTS

This review covers a decade of pioneering studies of neutron scattering from amorphous polymers. In the first five years the work was done with low flux neutron beams and spectrometers of low resolution. A major advance occurred with the commissioning of the high flux beam reactor at the ILL in Grenoble and its new generation of instruments which offered higher resolution and made accessible a wider range of momentum transfer values. Within the next year the new spin-echo spectrometer is expected to add a further two orders of magnitude to the low values of Q available. This machine will be of crucial importance in extending the quasi-elastic scattering studies of polymer chain dynamics.

In the next decade the major event will be the commissioning by SRC of the new spallation source at the Rutherford Laboratory. This will provide an even more intense beam of pulsed neutrons and will be associated with another generation of new spectrometers. The prognosis is that it will be particularly useful in time-resolved small-angle neutron scattering studies of polymers and for studies of the dynamics of polymer chains.

So far neutron scattering studies have been concentrated on problems in polymer science. As facilities develop these techniques will be applied to problems in polymer technology. Preliminary experiments are under way but by their very nature they are more protracted than pure science studies. The first results on stress relaxation, mixing and extrusion problems can be expected in the next two years.

ACKNOWLEDGEMENTS

The authors would like to thank Professor G. Allen for all his help and encouragement during the preparation of this review. Thanks are also due to AERE Harwell for providing an EMR grant for one of us (R. W. R.).

REFERENCES

1 Egelstaff, P. A. 'Thermal Neutron Scattering'. Academic Press, London, 1965
2 Willis, B. T. M. 'Chemical Applications of Thermal Neutron Scattering'. Oxford University Press, Oxford, 1973
3 Bacon, G. E. 'Neutron diffraction' Clarendon Press, Oxford, 1967
4 Marshall, W. and Lovesey, S. W. 'Theory of Thermal Neutron Scattering' Clarendon Press, Oxford, 1971
5 Turchin, V. E. 'Slow Neutrons' Israel Program for Scientific Translations, Jerusalem, 1965
6 Allen, G. and Higgins, J. S. *Rep. Prog. Phys.* 1973, **36**, 1073
7 Van Hove, L. *Phys. Rev.* 1954, **95**, 249
8 Harryman, M. B. M. and Hayter, J. AERE Harwell Report, RRL 73/25
9 Schmatz, W., Springer, T., Schelten, J. and Ibel, K. *J. Appl. Crystallogr.* 1974, **7**, 96
10 A similar spectrometer is described in: Bunce, L. J., Harris, D. H. C. and Stirling, G. C. UKAEA Report, Harwell R6246
11 Douchin, F., Lechner, R. E. and Blanc. Y. ILL Internal Scientific Reports, ITR 26/73
12 Birr, M., Heidemann, A. and Alefeld, B. *Nucl. Instrum. Methods* 1971 **95**, 435
13 Ober, R., Cotton, J. P., Farnoux, B. and Higgins, J. S. *Macromolecules* 1974, **7**, 634
14 Kratky, O. *Pure Appl. Chem.* 1966, **12**, 483
15 Zimm, B. H. *J. Chem. Phys.* 1948, **16**, 1093
16 Huglin, M. B. *Pure Appl. Chem.* 1977, **49**, 929
17 Kirste, R. G. and Wunderlich, W. *Z. Phys. Chem.* 1968, **88**, 133
18 Hayashi, H., Hamada, F. and Nakajima, A. *Macromolecules* 1974, **7**, 959
19 *Ibid.* 1976, **9**, 543
20 Higgins, J. S. in 'Neutron Scattering in Materials Science' (Ed. G. Kostorz.) 1978, to be published
21 Richards, R. W. in 'Developments in Polymer Characterisation' (Ed. J. V. Dawkins) Applied Science, to be published 1978
22 Flory, P. J. 'Principles of Polymer Chemistry', Cornell University Press, Ithaca, New York, 1953
23 Cotton, J. P., Decker, D., Benoit, H., Farnoux, B., Higgins, J. S., Jannink, G., Ober, R., Picot, C. and des Cloizeaux, J. *Macromolecules* 1974, **7**, 863
24 Ballard, D. G. H., Wignall, G. D. and Schelten, J. *Eur. Polym. J.* 1973, **9**, 965
25 Wignall, G. D., Ballard, D. G. H. and Schelten, J. *Eur. Polym. J.* 1974, **10**, 801
26 Kirste, R. G., Kruse, W. A. and Schelten, J. *Makromol. Chem.* 1973, **162**, 299
27 Schelten, J., Kruse, W. A. and Kirste, R. G. *Kolloid Z. Z. Polym.* 1973, **251**, 919
28 Kirste, R. G. and Lehnen, B. R. *Makromol. Chem.* 1976, **177**, 1137
29 Genannt, R., Pechhold, W. and Grossmann, H. P. *Colloid Polym. Sci.* 1977, **225**, 285
30 Allen, G. and Maconnachie, A. unpublished results
31 Herchenröder, P. and Dettenmaier, M. results presented at *Low-Angle Neutron Scattering from Polymers Meeting, Imperial College, London*, July 1977
32 Schelten, J., Ballard, D. G. H., Wignall, G. D., Longman, G. and Schmatz, W. *Polymer* 1976, **17**, 751
33 Kruse, W. A., Kirste, R. G., Haas, J., Schmitt, B. J. and Stein, D. J. *Makromol. Chem.* 1976, **177**, 1145
34 Ballard, D. G. H., Rayner, M. G. and Schelten, J. *Polymer* 1976, **17**, 640
35 Allen, G., Higgins, J. P. and Yip, W. unpublished results
36 Kirste, R. G., Kruse, W. A. and Ibel, K. *Polymer* 1975, **16**, 120
37 Yoon, D. Y. and Flory, P. J. *Polymer* 1975, **16**, 645
38 Yoon, D. Y. and Flory, P. J. *Macromolecules* 1976, **9**, 299
39 Ballard, D. G. H., Rayner, M. G. and Schelten, J. *Polymer* 1976, **17**, 349
40 Gupta, A. K., Cotton, J. P., Marchal, E., Burchard, W., and Benoit, H. *Polymer* 1976, **17**, 363
41 Moan, M. and Wolff, C. *Polymer* 1975, **16**, 776
42 Cotton, J. P. and Moan, M. *J. Phys. (Paris) Lett.* 1976, **37**, 75
43 Katchalsky, A. *Pure Appl. Chem.* 1971, **26**, 327
44 de Gennes, P. G., Pincus, P. and Velasco, R. M. *J. Phys. (Paris)* 1976, **37**, 1461
45 Benoit, H. and Froelich, D. in 'Light Scattering from Dilute Polymer Solutions' (Ed. M. B. Huglin) Academic Press, London, 1972, Ch. 11
46 Duval, M., Duplessix, R., Picot, C., Decker, D., Rempp, P., Benoit, H., Cotton, J. P., Jannink, G., Farnoux, B. and Ober, R. *J. Polym. Sci. (Polym. Lett. Edn)* 1976, **14**, 585
47 Han, C. C. and Mozer, B. *Macromolecules* 1977, **10**, 44
48 Semylen, J. A., Dodgson, K., Higgins, J. S., Scales, L. E. and Wright, P. V. Presented at meeting on *Statistical and Dynamic Behaviour of Chain Molecules, Oxford,* 1977
49 Casassa, E. F. *J. Polym. Sci. (A)* 1965, **3**, 605
50 Benoit, H., Duplessix, R., Ober, R., Daoud, M., Cotton, J. P., Farnoux, B. and Jannink, G. *Macromolecules* 1975, **8**, 451
51 Picot, C., Duplessix, R., Decker, D., Benoit, H., Boué, F., Cotton, J. P., Daoud, M., Farnoux, B., Jannink, G., Nierlich, M., de Vries, A. J. and Pincus, P. *Macromolecules* 1977, **10**, 436
52 Boué, F, presented at the conference cited in ref 31
53 Allen, G., Maconnachie, A. and Richards, R. W. unpublished results
54 Singleton, R. W. *PhD Thesis* University of Manchester, 1977
55 Edwards, S. F. *Proc. Phys. Soc.* 1966, **88**, 265
56 Edwards, S. F. *J. Phys. (A)* 1975, **8**, 1670
57 des Cloizeaux, J. *J. Phys. (Paris)* 1975, **36**, 281
58 de Gennes, P. G. *J. Phys. (Paris) Lett.* 1975, **36**, 55
59 Moore, M. A. *J. Phys. (Paris)* 1977, **38**, 265
60 Daoud, M. and Jannink, G. *J. Phys. (Paris)* 1976, **37**, 973
61 Ma, S. K. 'Modern Theory of Critical Phenomena' Benjamin, Reading, Massachusetts, USA
62 Daoud, M., Cotton, J. P., Farnoux, B., Jannink, G., Sarma, G., Benoit, H., Duplessix, R., Picot, C. and de Gennes, P. G. *Macromolecules* 1975, **8**, 804
63 Cotton, J. P., Nierlich, M., Boué, F., Daoud, M., Farnoux, B., Jannink, G., Duplessix, R. and Picot, C. *J. Chem. Phys.* 1976, **65**, 1101
64 Richards, R. W., Maconnachie, A. and Allen, G. *Polymer* 1978, **19**, 266
65 Richards, R. W., Maconnachie, A. and Allen, G. unpublished results
66 Edwards, S. F. and Jeffers, E. to be published
67 Rouse, P. E. *J. Chem. Phys.* 1953, **21**, 1272
68 Zimm, B. H. *J. Chem. Phys.* 1956, **24**, 269
69 de Gennes, P. G. *Physics* 1967, **3**, 37
70 Dubois-Violette, E. and de Gennes, P. G. *Physics* 1967, **3**, 181
71 Akcasu, Z. and Gurol, H. *J. Polym. Sci. (Polym. Phys. Edn)* 1976, **14**, 1
72 Akcasu, Z. and Higgins, J. S. *J. Polym. Sci. (Polym. Phys. Edn)* 1977, **15**, 1745
73 Jannink, G. and St James, D. *J. Chem. Phys.* 1968, **49**, 486
74 Bueche, P. *J. Chem. Phys.* 1954, **22**, 603
75 Jannink, G. and Summerfield, G. C. IAEA–SM–155/C–2
76 Jannink, G. and de Gennes, P. G. *J. Chem. Phys.* 1968, **48**, 2260
77 de Gennes, P. G. *Macromolecules* 1976, **9**, 587, 594
78 Brochard, F. and de Gennes, P. G. to be published
79 Pincus, P. *Macromolecules* 1977, **10**, 210
80 Allen, G., Brier, P. N., Goodyear, G. and Higgins, J. S. *Faraday Symp. Chem. Soc.* 1972, **6**, 169
81 Maconnachie, A., Vasudevan, P. and Allen, G. *Polymer* 1978, **19**, 33
82 Allen, G., Higgins, J. S. and Wright, C. J. *J. Chem. Soc. Faraday Trans 2* 1974, **70**, 348
83 Allen, G., Ghosh, R. E., Heidemann, A., Higgins, J. S. and Howells, W. S. *Chem. Phys. Lett.* 1974, **27**, 308
84 Higgins, J. S., Ghosh, R. E. and Howells, W. S. *J. Chem. Soc. Faraday Trans. 2* 1977, **73**, 40
85 Larsson, K. E. *Faraday Symp. Chem. Soc.* 1972, **6**, 167
86 Singleton, R. *PhD Thesis* University of Manchester, 1977

87 Allen, G., Ghosh, R., Higgins, J. S., Cotton, J. P., Farnoux, B., Jannink, G. and Weill, G. *Chem. Phys. Lett.* 1976, **38**, 577
88 Higgins, J. S., Ghosh, R. E., Allen, G., Farnoux, B. and Weill, G. *Chem. Phys. Lett.* submitted for publication
89 Sauer, J. A. *J. Polym. Sci. (C)* 1971, **32**, 69
90 Saito, N., Okono, S., Iwayanagi, S. and Hideshina, T. *Solid State Phys. Adv. Res. Appl.* 1963, **14**, 344
91 Woodward, A. E. *Pure Appl. Chem.* 1966, **12**, 341
92 McCall, D. W. in 'Molecular Dynamics and Structure of Solids' (Eds. R. S. Carter and J. J. Rush) NBS Special Pub. 301, Washington, 1969
93 Boutin, H. and Yip, S. 'Molecular Spectroscopy with Neutrons' MIT Press, Cambridge, Massachusetts, 1968
94 Gordon, R. J. *J. Chem. Phys.* 1965, **43**, 1307
95 Brier, P. N., Higgins, J. S. and Bradley, R. H. *J. Mol. Phys.* 1971, **21**, 721
96 Kittel, C. K. 'Introduction to Solid State Physics' Wiley, New York, 1971
97 Cunliffe, A. V., in 'Internal Rotations in Molecules' (Ed. W. J. Orville-Thomas) Wiley, London, 1974, Ch. 7
98 Allen, G. and Fewster, S. in 'Internal Rotations in Molecules' (Ed. W. J. Orville-Thomas) Wiley, London, 1974, Ch. 8
99 Higgins, J. S., Allen, G. and Brier, P. N. *Polymer* 1972, **13**, 157
100 Allen, G., Wright, C. J. and Higgins, J. S. *Polymer* 1974, **15**, 319
101 Herschbach, D. R. *J. Chem. Phys.* 1959, **31**, 91
102 Frossini, V. and Woodward, A. E. *J. Polym. Sci. (A-2)* 1969, **7**, 525
103 Townes, C. H. and Shawlow, A. L. in 'Microwave Spectroscopy' McGraw–Hill, London, 1955, Ch. 12
104 Harmony, M. D. *Chem. Soc. Rev.* 1972, **1**, 211
105 Williams, J., Shohomy, E., Reich, S. and Eisenberg, A. *Phys. Rev. Lett.* 1975, **35**, 95
106 Eisenberg, A. and Reich, S. *J. Chem. Phys.* 1969, **51**, 5706
107 Stejskol, E. O. and Gutowsky, H. S. *J. Chem. Phys.* 1958, **28**, 388
108 Yono, O. and Wada, Y. *J. Polym. Sci. (A-2)* 1971, **9**, 669
109 Froix, M. F., Williams, D. J. and Goedde, A. O. *Macromolecules* 1976, **9**, 354
110 Hägele, P. C. and Beck, L. *Macromolecules* 1977, **10**, 213
111 Spells, S. J., Shepherd, I. W. and Wright, C. J. *Polymer* 1977, **18**, 905
112 Wright, C. J. in 'Structural Studies of Macromolecules by Spectroscopic Methods' (Ed. K. J. Ivin) Wiley, London, 1976, Ch. 3
113 Kim, J. J., McLeish, J., Hyde, A. J. and Bailey, R. T. *Chem. Phys. Lett.* 1973, **22**, 503
114 Allen, G. and Richards, R. W. unpublished data
115 Zoller, P., Fehl, D. L. and Dillinger, J. R. *J. Polym. Sci. (Polym. Phys. Edn)* 1973, **11**, 1441
116 Allen, G. and Wright, C. J. Appendix to 1975 SRC Neutron Beam Committee Annual Report, p. 201